Indoor Radio Propagation Modelling with Antenna Placement Optimization

Fabian Ågren

master's thesis

March 2017

Lund University

Faculty of Science
Centre for Mathematical Sciences
Mathematical Statistics

Abstract

The use of wireless communication has grown rapidly over the last three decades. The Swedish Post and Telecom Authority estimates that more than 80% of all mobile traffic is received or transmitted from within buildings and the number is expected to reach over 90% in the near future. Meanwhile, the number of energy efficient buildings on the Swedish housing market has increased. This type of buildings blocks nearly all electromagnetic waves and makes it difficult to rely on outdoor antennas to provide sufficient coverage indoors. Subsequently, the need for indoor antenna systems has arisen.

In this master's thesis, a new antenna placement optimization algorithm is proposed. The algorithm aims to minimize the number of antennas required to provide sufficient indoor coverage, thus minimizing the cost of equipment and installation work. The semi-deterministic dominant path model was utilized by the optimization algorithm to predict coverage. Finding the most adequate dominant paths is essential to get accurate predictions using the dominant path model. This master's thesis proposes a new method of finding the dominant path by employing the path finding algorithms, A* and Θ*. The resulting algorithms were tested and evaluated at three test sites.

Acknowledgements

I would like to express my gratitude to my supervisor Andreas Jakobsson for encouraging this thesis and for his guidance and valuable opinions. Thanks go to North Net Connect and my co-supervisor Johan Jober for the idea of the master's thesis and their support. I would like to thank Johan Swärd for the support with developing the optimization algorithm and I would also like to express my appreciation to Tove Rydén Sonesson for proofreading and help with constructing figures.

I would like to offer my special thanks to Tommy Lundgren at HI3G Access for providing equipment and software and for his support and opinions.

Contents

Chapter 1

Introduction

1.1 Background

The use of wireless communication for personal and commercial use has grown rapidly over the last three decades. More devices than ever can communicate over radio frequencies. Combined with an increasing demand of high quality services, such as streaming high resolution video, calls for a well-planned and optimized network.

The Swedish Post and Telecom Authority (PTS) estimates that more than 80% of all mobile traffic is received or transmitted from within buildings and the number is expected to reach over 90% in the near future. PTS also concludes that more than 50% of all telephone calls are made through mobile devices and that the majority of the use of mobile data communication services, such as UMTS and LTE, are made indoors. Moreover, 30% of all Swedes rely solely on mobile phones for making calls and, consequently, have no access to traditional communication techniques, i.e. landlines [25].

In Sweden, most of the radio coverage indoors comes from base stations placed outside. If the penetration of radio waves through the building walls is good, the end user will experience full services. However, in the opposite case when the waves cannot penetrate sufficiently, the end user will experience poor services or, at worst, the use of radio devices will be impossible. As energy efficient buildings have been introduced to the Swedish housing market in recent years, an issue regarding the indoor radio coverage has arisen [1]. Good isolation and energy windows has proven to be an efficient damper of radio waves and is now a major cause of poor indoor coverage. This type of buildings reflect nearly all electromagnetic waves and makes it difficult to rely on outdoor antennas to provide good or even descent coverage indoors. Furthermore, recently imposed European Union regulations state that all new buildings shall be energy efficient as of the end of 2020. The issue of poor indoor radio coverage is thus likely to increase within the European Union over the coming years [24]. Consequently, new solutions need to be developed to meet the future demand of indoor mobile device usage.

1.1.1 Solutions for indoor coverage

Repeaters and base stations

The search for new technology to improve the indoor coverage has resulted in a few solutions that have been tested and evaluated. One of them is repeaters. Repeaters are often installed on the exterior of a building and their main task is to receive the signal from the closest outdoor base station and retransmit it using antennas mounted indoors. It also works in the opposite direction, i.e., it receives signals from mobile devices inside the building and retransmits them back to the outdoor base station. One of the main challenges with repeaters is the importance of installing them correctly. It must be performed correctly or the repeters may interfere with the general mobile network outside. If the interference is severe, this might even block calls to emergency services. An alternative to the use of repeaters is to dedicate a base station to each building. This is then often placed inside the building and is then connected to antennas within the building [25].

Distributed antenna systems

Regardless of whether a repeater or a base station solution is chosen, the signal must still be distributed to all areas inside the building. This can be done using a *distributed antenna system* (DAS). The DAS is an infrastructure consisting of cables, hardware, and antennas, which has the task to transfer signals throughout the building. An example of a DAS system can be seen in figure 1.1. Three exterior antennas are placed on the roof of the building and the signal is fed to a repeater placed in the basement. The repeater in turn repeats the signal and feeds it to distributed antennas placed on every floor including the basement.

DASs connected to repeaters or base stations can improve the coverage indoors considerably but they come at a cost. The infrastructure needed for the DAS is expensive, at least in the sense of costs compared to the expected number of users. As a consequence distributed antenna systems are often limited to larger buildings such as shopping malls, larger apartment buildings and business complexes. Furthermore, the placement of the interior antennas are of importance, not only for good coverage but also to minimize the interference on the radio network outside the building. This is not an issue if the exterior walls are good blockers of the radio waves [25].

Wi-Fi

Due to the high cost of DAS relative to the number of users, focus has been switched to a commonly existing indoor radio network infrastructure, namely Wi-Fi. Wi-Fi can be advantageous compared to previous technology since the access points needed are commodity hardware, i.e., it is easy to install and in most cases professional help is not require to do so. Wi-Fi antennas are often present in modern homes and companies, and no additional hardware therefore needs to be installed in order to use it as a communication source. Wi-Fi networks also operates at other frequencies than regular mobile traffic,

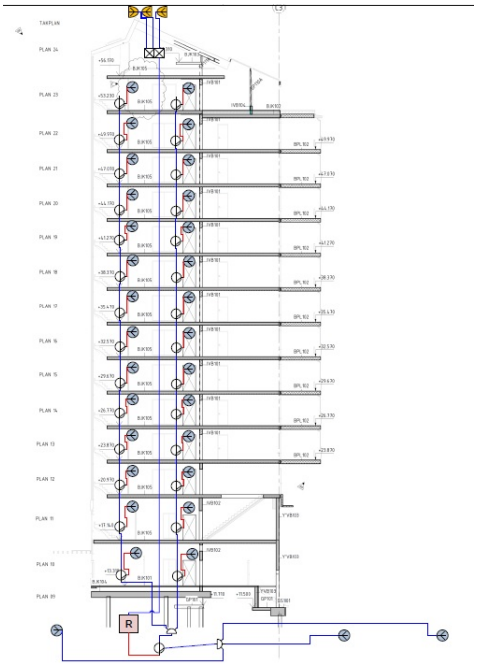

Figure 1.1: An example of a distributed antenna system (DAS) connected to a repeater placed in the basement.

resulting in zero interference with the mobile network. However, Wi-Fi networks are mainly developed to handle data communication and not traditional services such as phone calls and text messaging. As technology progresses in the future, this will probably change. Text messages have, in some sense, already been challenged by applications such as Facebook Messenger and voice calls over the internet protocol have been around for a couple of years with applications such as Microsoft Skype and Facebook Messenger. Recently, a new generation telecommunication system has been developed to support mobile voice, data, and multimedia over internet protocol networks, namely Wi-Fi calling. Wi-Fi calling makes the use of third party applications unnecessary when calling using internet protocol networks [12].

A disadvantage of Wi-Fi networks is that antennas are mainly controlled by the consumers. In densely populated areas, such as apartment buildings, interference between local networks is often inevitable as every consumer installs their own access points with no regards to their neighbours. Uncoordinated Wi-Fi transmitters prevents the full potential of the network. To prevent this issue, one recent solution is to build so called carrier Wi-Fi networks. Instead of referring the responsibility of managing Wi-Fi networks to the consumers, the property owner builds a coordinated network. All the residents then share the available antennas. Carrier networks make it possible to reduce interference and efficiently provide coverage throughout the building [25].

1.1.2 Network planning

Today, when implementing a radio network indoors, antenna placement is often based on the experience of the radio planner. Though software assisting antenna placement is available on the market, they are usually expensive and sometimes overly sophisticated [1] [2].

When implementing a Wi-Fi network or a distributed antenna system in large buildings such as shopping malls, apartment buildings, train stations, airports or office complexes, it is important to plan the network properly to get good coverage. The placement of the antennas are critical in order to optimize the network. In an existing building, this parameter is often limited to practical conditions such as where the wall sockets are located as well as aesthetic characteristics of visible or non-visible antennas. The range of antennas used in Wi-Fi and DASs are strictly limited. The outputted power of Wi-Fi antennas is restricted by legal regulations in most countries [2], whereas DAS antennas are instead limited as they need to not interfere with the mobile network outside the building [25]. Because of the limited range, more antennas are needed to provide sufficient coverage. However, more antennas will necessitate more cables, additional hardware and consequently generate higher costs. Even though for instance Wi-Fi hardware and antennas are relatively cheap today, the number of access points required to cover large buildings can be considerable. Significant savings could be made if parts of the used access points could be removed without reduction of the network quality.

1.2 Problem formulation

A question that often arises when planning a network in residential buildings is: if an antenna is put in a staircase, will it be able to provide coverage to all apartments on the current floor? In cases like this, accuracy, i.e., how strong the received signal will be, is not the primary concern. Rather, the relevant question is whether the required coverage is provided or not. Such answers can be provided by advanced techniques, using ray-trace models, but it would be preferable if one could move such conditions without resorting to such methods.

This master's thesis was initiated to investigate if there are simple radio propagation models that are able to provide a good answer to questions such as the one above. It is also desirable to investigate if such propagation models can be used to suggest appropriate locations of the antennas to ensure sufficient coverage. As the current practice of radio planning indoors is experience based, i.e., the placement of antennas is based on the knowledge and experience of the radio planner, a key feature of the chosen propagation model should be its simplicity.

1.2.1 Aim

The aim of this master's thesis is divided into two parts.

[1] Tommy Lundgren, radio planner, HI3G Access, personal communication, August 27, 2016.
[2] Johan Jober, CTO, North Net Connect, personal communication, June 22, 2016.

1. The first part is to find an existing radio propagation model that can predict the *received signal strength* in a given point in an indoor environment, given the locations of the antennas. The propagation model is not required to predict precise values of the received signal strength with high precision, rather the model should allow for a reliable prediction as to tell whether or not a given point will have sufficient coverage. Since the propagation model should be pertinent, it must balance low computational load and accuracy loss well. It must also be fairly independent of building details. In the ideal case, the model would only require a simple floor plan to generate accurate predictions.

2. The second aim is to use the established propagation models to minimize the number of antennas required in order to get a sufficient coverage in a given area. The solution to this optimization problem should thus yield a set of appropriate antenna locations.

1.3 Scope

Nearly all frequencies are of interest when planning a radio network. However, it is difficult to optimize an existing distributed antenna system since hardware, cables and antennas are not mobile. Hence, this master's thesis will only consider Wi-Fi networks and by that only frequencies in the 2.4 GHz band. The 5 GHz frequency band is excluded since mobile frequencies in Sweden are located closer to 2.4 GHz. The main advantages of working with Wi-Fi networks are the hardware, simplicity of moving antennas, and as well as the abundance of software available to measure signal strength.

Radio signals propagate in all directions in the three-dimensional space. Not only will they penetrate walls and objects, they also go through floors and ceilings. Although it is clear that some radio waves will penetrate floors and contribute to the received signal strength, this effect may be excluded to construct easier models. Consequently, the thesis only consider the two-dimensional case.

1.4 Thesis outline

This thesis is organized as follows:

Chapter 1	This chapter introduces the background of the master's thesis by covering the basis of network implementation and planning. The background makes up the foundation of the problem formulation which is also presented in the chapter.
Chapter 2	The next chapter gives a brief introduction to radio propagation modelling. It then introduces four different radio propagation models developed especially for indoor applications.

Chapter 3	This chapter deals with the implementations of the propagation models described in the previous chapter.
Chapter 4	This chapter evaluates all the propagation models described and implemented in chapter 2 and 3, respectively. It covers the theory of estimating the model parameters as well as how to analyse the result.
Chapter 5	This chapter addresses the antenna placement optimization part of the thesis. The optimization problem is formulated and an antenna placement selection algorithm is presented and tested.
Chapter 6	The final chapter discusses the results obtained in the thesis. It also suggests further development and improvements.

Chapter 2

Propagation Models and Theory

There are plenty of radio propagation models available, of which many have been developed to predict signal strength in indoor environments. Propagation models can mainly be divided into three categories: *empirical models*, *deterministic models*, and *semi-deterministic models* [17]. Empirical models are based on observations of the channel and are often formulated as simplified mathematical formulas. Its parameters are fitted to a data set of channel measurements collected from indoor environments similar to the modelled environment. Thus, empirical models generally have low computational load but since they do not take specific propagation details into account, they lack good accuracy. By contrast, deterministic models, which generally are based on Maxwell's equations, are very dependent on the propagation environment and require accurate details about the environment in order to perform well. The deterministic models have high computational load which make them less preferable in the context of this thesis. Semi-deterministic models are a trade-off between empirical and deterministic models. They are expressed as simplified mathematical formulas with some of the parameters based on the specific propagation environment. These models have been proven to improve the accuracy compared to empirical models and still retain low computational load [27].

2.1 Units

The received signal strength is measured in watts (W). However, the signal power is known to vary considerably. As this variation can range several orders of magnitude, it is impractical to use a linear scale. Thus, it is often more convenient to express the power as a ratio compared to a base line of 1 milliwatt. The ratio is expressed in the dimensionless unit decibel (dB). In this way, the power P_{w} expressed in milliwatts (mW) can be expressed in a logarithmic scale as

$$P_{\mathrm{dBm}} = 10 \log_{10} \left(\frac{P_{\mathrm{w}}}{1\,\mathrm{mW}} \right) \tag{2.1}$$

which is thus expressed in the dimensionless unit decibel-milliwatts (dBm). A signal power of 0 dBm corresponds to 1 mW and a decrease of power with 10 dBm means that the power has been reduced 10 times its previous value. The formula to convert from dBm to mW is

$$P_{\mathrm{w}} = 10^{\frac{P_{\mathrm{dBm}}}{10}}. \tag{2.2}$$

2.2 Free space model

Before introducing propagation models for indoor use, it is worth taking a closer look at models for radio propagation in free space. The free space path loss model is possibly the simplest model in the field of radio propagation. It describes to what extent the signal strength of an electromagnetic wave has diminished at a certain distance from the transmitter in the absence of obstacles. The model is based on Friis' transmission equation, which states that the received power, P_r, at a receiving antenna with antenna gain G_r is

$$P_r = P_t G_t G_r \left(\frac{\lambda}{4\pi d}\right)^2 \tag{2.3}$$

where P_t is a outputted power from a transmitting antenna and G_t is its gain [22]. The parameter λ is the wavelength of the electromagnetic wave and d is the straight-line distance between the location $\mathbf{x}$ of the transmitting antenna and the location $\mathbf{p}$ of the receiving antenna, more formally defined as

$$d = ||\mathbf{x} - \mathbf{p}||_2 \tag{2.4}$$

Power is expressed in watts (W) but as mentioned in section 2.1, it is often convenient to express power in decibels instead. In that case, Friis' equation is modified to

$$P_r|_{dBm} = P_t|_{dBm} + G_t|_{dBi} + G_r|_{dBi} + 20\log_{10}\left(\frac{\lambda}{4\pi d}\right) \tag{2.5}$$

with power now being expressed in decibel-milliwatts (dBm) and the gain in decibel-isotropic (dBi). If the transmitting and receiving antenna are assumed to be isotropic, i.e., broadcasting and intercepting an equal amount of energy in all directions, the antenna gains can be excluded. An isotropic antenna is purely hypothetical and can not be constructed in reality. Nevertheless, they can be adopted in modelling in order to simplify the use of the propagation model. With these assumptions, the ratio of the antenna gains are equal to one, which in logarithmic scale is equivalent to

$$G_t|_{dBi} = G_r|_{dBi} = 0. \tag{2.6}$$

This simplifies Friis' equation to

$$P_r|_{dBm} = P_t|_{dBm} + 20\log_{10}\left(\frac{\lambda}{4\pi d}\right). \tag{2.7}$$

The path loss, L, which is the difference between transmitted power and received power is then

$$\begin{aligned} L(d) = P_t|_{dBm} - P_r|_{dBm} &= 20\log_{10}\left(\frac{4\pi d}{\lambda}\right) \\ &= 20\log_{10}\left(\frac{4\pi}{\lambda}\right) + 20\log_{10}(d). \end{aligned} \tag{2.8}$$

Henceforth, the signal power will always be expressed in dBm in the thesis.

2.3 Signal fading

The free space model can be used as an efficient predictor for received signal strength in ideal conditions. However, in indoor environments there are many obstacles that weaken the signal strength. The signal will reflect, refract and diffract around walls, floors, furniture, human bodies and so forth. This causes the signal to fluctuate in a random manner. As a consequence, several rays from the transmitter will reach the receiver using different paths. This phenomena is referred to as multipath propagation. The effects of multipath propagation is destructive or constructive interference between different paths which makes the signal amplitude fluctuate rapidly over short distances.

Another cause of fading is shadowing. Shadowing occurs when the receiver is caught behind an obstacle relative to the transmitter, for example behind a corner or wall. This causes long-term random fluctuations in the received signal power. It is common to model shadowing as a random variable Ψ which follows a log-normal distribution with probability density function [19]

$$f_\Psi(\psi) = \frac{10}{\psi\sigma\pi\sqrt{2}\ln(10)} e^{-\frac{(10\log_{10}(\psi)-\mu)^2}{2\sigma^2}} \tag{2.9}$$

where μ is the mean and σ the standard deviation of Ψ, respectively. The effects of fading can make it challenging to model the received signal strength indoors, especially when empirical models are used.

2.4 Indoor propagation models

One of the important goals of this master's thesis is to find a radio propagation model suitable for prediction in indoor environments. It must also manage to make predictions within a reasonable time frame. Since deterministic models are known for their high computational load, the focus has been directed toward empirical and semi-deterministic models. This section presents the models that were selected for testing and evaluation.

2.4.1 One-slope model

The one-slope model is an empirical model inspired by the free space model in (2.8). It states that the path loss at a straight-line distance d from the

Table 2.1: Some typical values for the path loss exponent γ used in the one-slope radio propagation model [18].

Environment	**Path loss exponent** (γ)
inside a building - line-of-sight	1.6 - 1.8
free space	2
obstructed in a factory	2 - 3
obstructed in a building	4 - 6

transmitting antenna, defined in (2.4), is

$$L(d) = L_0 + 10\gamma \log_{10}(d) + X_\sigma \tag{2.10}$$

where L_0 is the path loss at a reference distance of 1 meter from the transmitter [9][17][4][27]. The path loss exponent γ describes the radio environment. It is typically calculated from measurements in some similar locations. The random variable X_σ with standard deviation σ models the random attenuation of the signal. The corresponding random variable

$$Z = 10^{\frac{X_\sigma}{10}} \tag{2.11}$$

which expresses the gain in watts may be modelled as a log-normal random variable if only shadowing is present. If multipath effects are present with no shadowing, then the random variable might instead be better modelled as following a Rayleigh or Ricean probability distribution [3][15].

When dealing with Wi-Fi antennas, the outputted power is often not known. Manufacturers of Wi-Fi access points do not usually provide details about the exact power, making it difficult to set the L_0-parameter in (2.10). Because Wi-Fi antennas are the preferred choice in this thesis, the one-slope model is slightly modified to overcome this issue. The introduced modification is

$$P_r(d) = P_{r|d_0} - 10\gamma \log_{10}(d) + X_\sigma \tag{2.12}$$

where $P_r(d)$ is the received signal strength at a straight-line distance d, as defined in (2.4). The parameter $P_{r|d_0}$ is the received signal strength at a reference distance of 1 meter from the transmitter and γ is, as before, the path loss exponent describing the radio environment.

The path loss exponent γ is in most cases not known. Therefore, it needs to be estimated from measurements or extracted from a similar environment where the exponent is known. Some possible values of γ can be found in table 2.1.

2.4.2 Dual-slope model

The attenuation of the signal can be influenced in varying degrees depending on if the propagation occurs in line-of-sight (LOS), i.e., there is a straight, not obstructed, path between the transmitter and the receiver, or in non-line-of-sight (NLOS) [9]. It seems reasonable to assume that the signal will decay

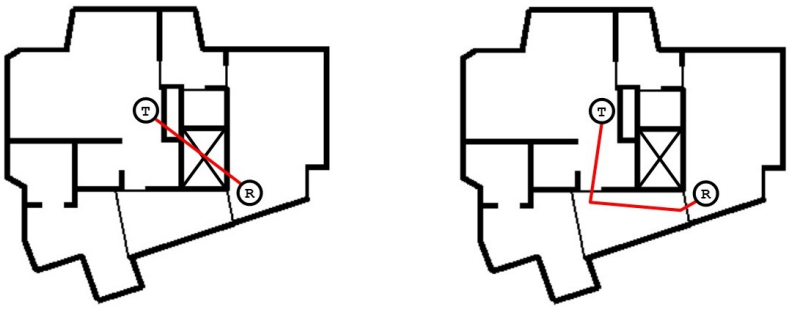

(a) (b)

Figure 2.1: The one-slope and dual-slope models are dependent on the direct path between the transmitter and the receiver, as seen in (a), even if the signal is unlikely to take this path. The dominant path model uses paths that go around obstacle for predictions, as seen in (b).

quicker in a NLOS scenario as compared to a LOS scenario. The dual-slope model uses two different slopes for LOS and NLOS and can be formulated as

$$P_r(d) = X_\sigma + \begin{cases} P_{r_1|d_0} - 10\gamma_1 \log_{10}(d), & \text{if LOS} \\ P_{r_2|d_0} - 10\gamma_2 \log_{10}(d), & \text{if NLOS.} \end{cases} \tag{2.13}$$

The path-loss exponents γ_1 and γ_2 are estimated from measurements from LOS and NLOS environments, respectively.

2.4.3 Dominant path model

The one-slope dominant path model is a semi-deterministic model proposed to enhance the accuracy of simple empirical models such as the one-slope model. The one-slope and dual-slope models assume a direct propagation path between the transmitter and the receiver. However, this is not likely to be true in indoor propagation environments. Consider the case shown in figure 2.1. The transmitter is placed in a room located in the upper left part of the building. The receiver is placed in the room to the far right. In between, an elevator shaft with concrete walls and metal cover is blocking the direct path, as seen in figure 2.1a. In this situation, empirical models based on the direct path are likely to miss this significant information and will predict the received signal strength inaccurately. A perhaps more likely scenario would be that most of the signal energy would go around the solid obstacle to reach the receiver as seen in shown 2.1b.

The dominant path model rely on the fact that in most situations, more than 90 percent of the signal energy will flow through not more than three rays between the transmitter and the receiver [10]. For instance, in figure 2.2, due to multipath effects, many rays will use different paths to reach the receiver. All the received rays are superimposed at the receiver to reconstruct the sent signal. However, it is likely that the rays, shown as being solid lines, will carry most of the signal energy since its path does not penetrate many obstacles that will

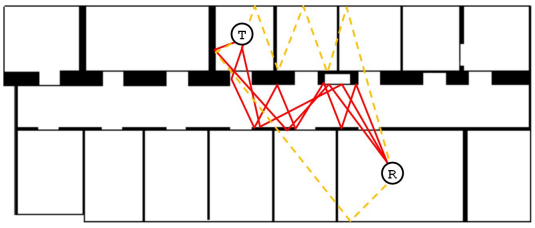

Figure 2.2: Multiple rays reach the receiver by different paths. The dashed rays will be attenuated more than the solid ones.

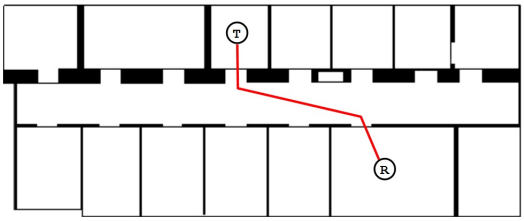

Figure 2.3: The dominant path model approximates the rays carrying the most energy by one dominant path.

attenuate the signal. In contrast, the dashed rays will be highly attenuated due to the number of walls that are penetrated. The idea is to approximate the rays that carry most of the signal energy and replace them with one dominant path as seen in figure 2.3. The dominant path found is used as input to the model. The dominant path is defined by N waypoints between a transmitter located at $\mathbf{x}_1$ and a receiver located at $\mathbf{x}_N$ every location $i \notin \{1, N\}$ indicates a location where the path changes direction. Then, the length d_{dom} of the dominant path is

$$d_{dom} = \sum_{i=1}^{N-1} ||\mathbf{x}_{i+1} - \mathbf{x}_i||_2 \tag{2.14}$$

The predicted received signal strength is calculated based on the dominant path using the one-slope model as

$$P_r(d_{dom}) = P_{r|d_0} - 10\gamma \log_{10}(d_{dom}) + X_\sigma. \tag{2.15}$$

The dominant path model has been showed to significantly improve the accuracy as compared to simple empirical models [10][27]. The complexity in the model lies in computing the dominant path. One proposed way of computing them is by using machine learning techniques taking in consideration the geometry of the rooms [26]. However, machine learning requires a lot of data in order to get good results. In this thesis we aim to find a good on-line method to calculate the dominant paths which also can do it fast enough. This is proposed in the next chapter.

2.4.4 Dual-slope dominant path model

The dual-slope dominant path model is the LOS and NLOS extension of the dominant path model. It is formulated as

$$P_r(d_{dom}) = X_\sigma + \begin{cases} P_{r_1|d_0} - 10\gamma_1 \log_{10}(d_{dom}), & \text{if LOS} \\ P_{r_2|d_0} - 10\gamma_2 \log_{10}(d_{dom}), & \text{if NLOS.} \end{cases} \tag{2.16}$$

where the parameters have the same purpose as in the dual-slope model.

Chapter 3

Dominant paths

In the previous chapter two empirical and two semi-deterministic propagation models for indoor environments were studied. Two of them, the one and two-slope dominant path models, are dependent on an approximation of the highest energy carrying rays, called dominant path. In this chapter, a new method of finding dominant paths will be introduced. The method proposed contains path-finding algorithms frequently used in the design of computer games and in robotics. Finding the most adequate dominant path as possible is essential in order to get accurate predictions using the dominant path model.

3.1 A* search algorithm

The A* search algorithm is a widely used algorithm in computer science for path finding and graph traversal, i.e., the process of finding an efficiently traversable path between points, called nodes. The algorithm was first proposed by Peter Hart, Nils Nilsson, and Bertram Raphael in 1968 [21] and has since been noted for its speed and accuracy. The algorithm is an extension of the famous Dijkstra's algorithm.

3.1.1 Dijkstra's algorithm

Dijkstra's algorithm has gotten its name after the Dutch computer scientist Edsger W. Dijkstra who conceived the algorithm in 1959 and published it three years later [8]. The algorithm is used to find the path associated with the least cost to traverse between two nodes in a given graph. It works by visiting adjacent nodes of the start node. It then selects the node with the lowest cost to visit and expands its adjacent neighbours. It then repeats the process by selecting the node that has lowest cost, calculated from the starting node, among all the expanded nodes. If the graph is a grid, then the algorithm will expand all nodes surrounding the starting node in a square shape until the goal node is reached. In this way, the Dijkstra's algorithm is guaranteed to find the path with the lowest cost. However, since Dijkstra's algorithm will expand every

possible node until the best path is found it can be rather slow, especially if the graph contains a large set of nodes and vertices.

3.1.2 Greedy best-fit-search

An alternative to Dijkstra's algorithm is the greedy best-fit-search algorithm. Greedy best-fit-search works in a similar way as Dijkstra's algorithm but instead of selecting nodes closest to the starting node, it selects nodes closest to the goal node for expansion. Because the optimal path is unknown, the greedy algorithm can never know for sure how close it is from the goal node. Instead, it uses some estimate to determine the distance left to the target. This estimate is usually referred to as a heuristic. Due to the heuristic, the greedy best-fit-search will only expand nodes towards the goal node, thus avoiding expansion towards nodes in the opposite direction relative to the goal node. Hence, the algorithm will generally be very fast compared to Dijkstra's algorithm. The main disadvantage of the greedy best-fit-search is that, since it uses a heuristic to determine the direction of expansion, it leaves no guarantee that the optimal path, or even a suboptimal path, will be found. For instance, when an obstacle is located in between the start and the goal node, the greedy best-fit-search algorithm might head right into it before finding a way around. Therefore, there is always a risk of detours when deploying the greedy best-fit-search algorithm [20].

3.1.3 The A* algorithm

The A* search algorithm combines Dijkstra's algorithm and the greedy best-fit-search to extract the best out of both algorithms, namely speed and accuracy. It does this by adding the cost of the path travelled, to the heuristic estimate of how far it has left. More formally, if n is the current node that is being examined and $g(n)$ is the cost to travel from the start node to n and $h(n)$ is the heuristic estimate of the distance between the current node and the goal node, then the A* search algorithm uses the function $f(n)$ defined as

$$f(n) = g(n) + h(n) \tag{3.1}$$

to evaluate which nodes to expand. Note that Dijkstra's algorithm is a special case of the A* search algorithm when no heuristic is used, i.e., $h(n) \equiv 0$, and greedy best-fit-search is the opposite case, when the travelled cost is neglected, i.e., $g(n) \equiv 0$. When the algorithm finds the goal node, it needs to backtrack the expanded nodes in order to find the path. This is accomplished by saving the parent of every node, i.e, where it came from during the traversal, and then traversing the graph backwards.

The A* search algorithm used in this master's thesis was implemented in Matlab from pseudo code printed in an article by K. Daniel et al. from the University of Southern California [11]. The pseudo code for the A* search algorithm is summarized below in Algorithm 1. Some brief notes about the algorithm; s_{start} is the start node and s_{goal} is the goal node. The set denoted "open" is the set of all nodes that has been expanded and are about to be checked. The set

Algorithm 1 A* search algorithm

```
1: procedure ASTAR
2:     g(s_start) := 0
3:     parent(s_start) := s_start
4:     open := ∅
5:     open.Insert(s_start, g(s_start) + h(s_start))
6:     closed := ∅
7:     while open ≠ ∅ do
8:         s := open.Pop
9:         if s = s_goal then return success
10:        closed := close ∪ {s}
11:        for each s' ∈ nghbrs(s) do
12:            if s' ∉ closed then
13:                if s' ∉ open then
14:                    g(s') := ∞
15:                    parent(s') := NULL
16:                UpdateVertex(s, s')
       return failed

17: procedure UPDATEVERTEX
18:    if g(s) + c(s, s') < g(s') then
19:        g(s') := g(s) + c(s, s')
20:        parent(s') := s
21:        if s' ∈ open then
22:            open.remove(s')
23:        open.Insert(s', g(s') + h(s'))
```

denoted "closed" is the set of all nodes that has been evaluated. The method "open.Insert" adds a node to the set with its corresponding estimate, as defined in (3.1). The method "open.Pop" retrieves and removes the node in the set "open", which minimizes $f(n)$. The method "nghbrs" retrieves a set containing all the adjacent neighbours of a node. The method "open.Remove" simply removes a node from the set "open", and c is the cost function which will be defined in the following equations, (3.8) and (3.9).

3.2 Floor plan format

A good radio propagation model must not only be fairly accurate and have low computational load, it must also be easy to use. Radio network planning indoors are typically experience based. Consequently, mathematical models are generally not utilized. The result might be unnecessarily oversized networks or individual receivers that lack proper coverage. To compete with experience based methods, a useful model should minimize the need for preparation by being able to make sufficient predictions without requiring more advanced input than a two-dimensional floor plan.

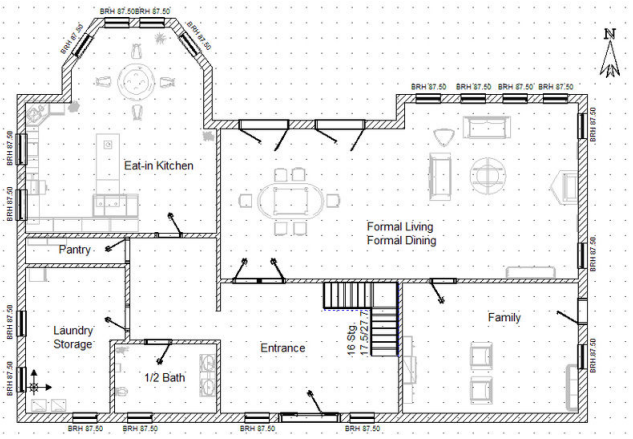

Figure 3.1: An example of a floor plan used to construct a binary image which is used in prediction [7].

Typically, more advanced models such as the ones based on ray-tracing require 3-dimensional floor-plan databases, including details of all obstacles etc., in order to work properly. Generally, it can be difficult to acquire such plans, if they exists for the building in question. Even if they do exist, small errors in the floor description can cause large deviations as ray-tracing models are very sensitive to changes. On the other hand, 2-dimensional floor plans, such as the one displayed in figure 3.1 often exist and are commonly digitalized.

It is common, especially in computer game design and robotics, to use a grid graph as base for the A* search algorithm. Every tile in the grid is considered a node and a node is generally connected to its four or eight adjacent neighbours, as shown in figure 3.2, depending on if diagonal movement is allowed. A grid is an intuitive way to discretize a two-dimensional space. If any tile represents a no-go zone it is disconnected from its neighbours. A natural representation of this kind of grid is a binary matrix where zeros represent free space and ones represent the no-go zones such as walls. An example of a simple binary image and its corresponding matrix can be seen in figure 3.3.

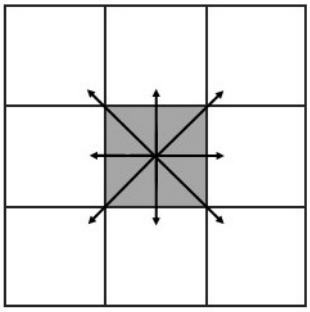

Figure 3.2: In a grid graph, every tile is considered a node and is often connected to its eight adjacent neighbours.

$$\begin{pmatrix} 1 & 1 & 1 & 1 & 1 & 1 & 1 & 1 \\ 1 & 0 & 0 & 1 & 1 & 0 & 0 & 1 \\ 1 & 0 & 0 & 1 & 1 & 0 & 0 & 1 \\ 1 & 0 & 0 & 1 & 1 & 0 & 0 & 1 \\ 1 & 0 & 0 & 0 & 0 & 0 & 0 & 1 \\ 1 & 1 & 1 & 1 & 1 & 1 & 1 & 1 \end{pmatrix} \Longrightarrow$$ 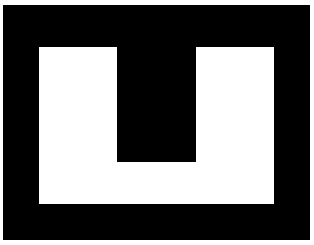

Figure 3.3: An example of a simple binary image representing a floor plan and its corresponding matrix. The ones in the matrix are representing walls and the zeros are free space. The figure is based on Giovanni Soldi's representation of binary grids [23].

The simplicity of a grid image and its compatibility with traditional path finding algorithms makes it an ideal floor plan format in this thesis. Regular floor plans are usually created in software based on computer-aided design (CAD) and it should therefore pose no difficulty to construct binary floor plans out of such plans.

3.3 The modified A* algorithm

The idea behind introducing the A* search algorithm in radio originates from Giovanni Soldi's masters thesis published in 2011 [23]. Soldi used the A* to enhance accuracy of positioning algorithms based on the received signal strength indoors where the GPS-coverage is poor. In this master's thesis, the A* search algorithm will be deployed to determine the dominant paths used in (2.15) and (2.16). Thus, the premise will be reversed; if the positions are known, what will the signal strength be?

Before A* can be deployed, some aspects regarding the material of the walls need to be resolved. Consider the case where a thick concrete wall is blocking the path between the transmitter and the receiver. The radio signal passing through the wall will be highly attenuated. If an alternative way around the wall exists, perhaps through a doorway a few meters away or an another wall made of a material with more favourable attenuation properties, then most of the energy might reach the receiver that way instead. However, if there is no such path available or the path available is too much of a detour, the dominant path might be through the concrete wall. The A* search algorithm should be able to determine which one it is. It seems proper to state the following definition of a dominant path in the discussed graphs.

Definition 1. *A dominant path between the nodes s_{start} and s_{goal} in a search graph is the path associated with the lowest cost to traverse.*

Dijkstra's algorithm will always find the dominant path, since it is guaranteed to find the path associated with the lowest cost. However, the computational time might be prolonged, especially for large grids. The A* search algorithm will also find the dominant path but at a faster pace as long as the heuristic

does not overestimate the cost of reaching the goal [6].

To account for the properties of the walls, the floor plan format has to be modified. Here, we propose to instead assigning a cost to every pixel in the floor plan image that represents how "easily" a radio wave enters the space represented by the pixel. The cost of traversing a material is then compared to the cost of traversing free space. In this thesis, the path loss in materials is approximated by a linear function over short distances, such that

$$L(d) = -\alpha d \tag{3.2}$$

where L is the path loss, d is the Euclidean distance of the path, and α is a an attenuation coefficient unique to the material, having dimensions m^{-1}. Free space, however, is a bit more tricky to approximate since the path loss varies a lot over large distances and is non-linear. However, to find a suitable cost, α, for pixels representing free space, the following observations may be made. If the length of one pixel corresponds to Δd meters, the path loss associated with traversing one pixel horizontally or vertically in free space may be expressed as

$$\begin{aligned}\Delta L(d) &= L(d + \Delta d) - L(d) \\ &= 20\log_{10}(d + \Delta d) - 20\log_{10}(d) = 20\log_{10}\left(1 + \frac{\Delta d}{d}\right)\end{aligned} \tag{3.3}$$

where d is the Euclidean distance between the n:th pixel's location, $\mathbf{p}_n$, and the transmitters location $\mathbf{x}$, i.e.,

$$d = ||\mathbf{p}_n - \mathbf{x}||_2. \tag{3.4}$$

The free space path loss of two common Wi-Fi frequency bands, namely 2.4 and 5 GHz, are displayed in figure 3.4a. After 30 meters, the path loss is around 70 dBm for the 2.4 GHz band and around 76 dBm for the 5 GHz band. Ergo, the signal will, in indoor environments, almost certainly be lost at this distance. Furthermore, the signal strength within a radius of 5 meters from the transmitter is generally not of interest since the coverage is then guaranteed to be good in most cases anyway. The differentiated free space path loss function, (3.3), is plotted in figure 3.4b. Most of the energy of the signals will spread out the first five meters, thereafter the energy will not decrease as fast.

In the light of the previous section, the interval between 5 and 30 meters can justifiably be used to estimate a constant representing the path cost in free space. The mean of the path loss per pixel may then be as an estimate of this cost. If the differentiated path loss function in (3.3) is discretized for every pixel n located at distances Δd, $2\Delta d$, $3\Delta d$, ... from the transmitter, it may be expressed

$$\Delta L(n\Delta d) = 20\log_{10}\left(1 + \frac{1}{n}\right). \tag{3.5}$$

Using the assumed range between 5 and 30 m implies that the function is sampled between $L = \lfloor \frac{5}{\Delta d} \rceil$ and $U = \lfloor \frac{30}{\Delta d} \rceil$, where $\lfloor x \rceil$ denotes the nearest integer function which rounds a real number x to nearest integer. In this case, the samples can be used to calculate the pixel mean path loss as

$$\mu_{\Delta d} = \frac{\Delta d}{25} \sum_{n=L}^{U} \Delta L(n\Delta d). \tag{3.6}$$

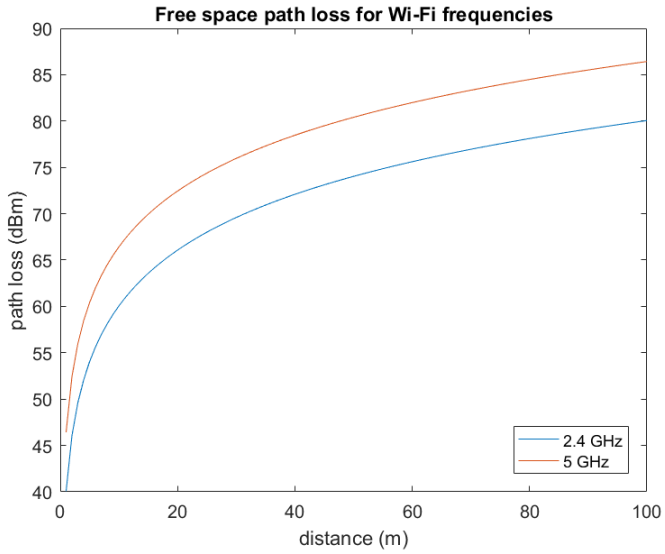

(a)

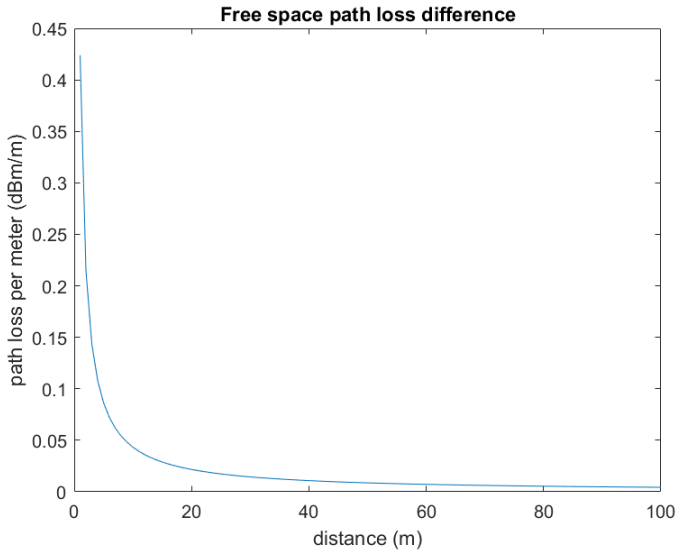

(b)

Figure 3.4: In (a), free space path losses for Wi-Fi frequencies 2.4 and 5 GHz. In (b), the differentiated path loss function of the path losses in (a). The derivative will be the same since they only differ by a constant.

The approximated linear path loss in free space per pixel is then normalized such that the cost c_n to traverse a pixel n with a certain medium in a grid is set to

$$c_n = \begin{cases} 1, & \text{if free space,} \\ \frac{\alpha}{\Delta d \mu_{\Delta d}}, & \text{if a material.} \end{cases} \tag{3.7}$$

Similarly, the total cost of moving into a pixel n from one of its adjacent neighbours n_{adj} is

$$g(n) - g(n_{\text{adj}}) = \varrho + c_n \tag{3.8}$$

if movement was made horizontally or vertically and

$$g(n) - g(n_{\text{adj}}) = \varrho\sqrt{2} + c_n \tag{3.9}$$

if movement was done diagonally, where ϱ is the basic cost of moving horizontally or vertically. ϱ is usually set to be one.

3.3.1 Simulation results

In order to test the algorithm, we proceed to test it on simulated data. The modified A* search algorithm was deployed on a binary image modified to the correct format, as described in the previous sections. The pixel width was selected as

$$\Delta d = 0.0562\,\text{m}. \tag{3.10}$$

Unfortunately, exact measurements of the attenuation of different materials were unavailable when this project was performed. As a replacement, standard values used in different radio design tools was used. A concrete wall will, according to the standard values, attenuate a signal at 2.4 GHz approximately 26 dBm, a standard window will attenuate the signal 4.4 dBm, and a energy efficient window will attenuate the signal 33.8 dBm [25]. The concrete walls at the test site were approximately 20 cm thick. Thus, an approximation of the attenuation coefficient, α, for a 20 cm thick concrete wall can be approximated by assuming that the attenuation of the wall will be 26 dBm. Consequently, the α-value used for a concrete wall will in the simulations be:

$$\alpha = 130 \quad \text{dBm/m} \tag{3.11}$$

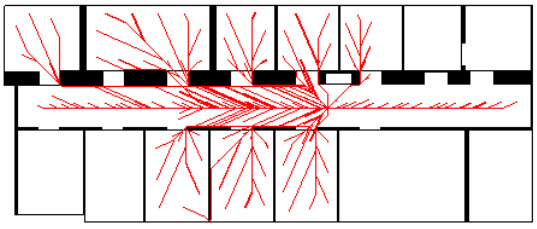

Figure 3.5: The A* search algorithm used to find dominant paths between one transmitter location and several potential receiver locations.

The heuristic used was the Euclidean distance

$$h(n) = \varrho\sqrt{(i_g - i)^2 + (j_g - j)^2} \tag{3.12}$$

where (i, j) is the coordinates of the current node n and (i_g, j_g) is the coordinates for the goal node. This heuristic is used as it is the shortest possible path left in reality between the current node n and the goal node. The multiplication by ϱ is done to weight h as compared to g.

As a simulation, many potential receiver locations were selected in an office corridor. Dominant paths were then found from one transmitter location to all the receivers using the A* search algorithm. The result of the simulation can be seen in figure 3.5.

3.4 Θ* search algorithm

Some well-known flaws of using the A* search algorithm for a grid based graph became clear during the simulations. The possible directions when travelling from a node to another is strictly limited to eight options: horizontal, vertical and diagonal movement. Consequantly, the paths might be longer than the corresponding paths in reality, as it is limited to the grid edges. It is desired to allow any possible heading in order to get realistic distances of the paths. An algorithm developed to manage this is the Θ* search algorithm. The Θ* search algorithm is an extension of the A* search algorithm which supports any-angle path finding. It was developed by Kenny Daniel, Alex Nash, Sven Koenig, and Ariel Felner in 2010. The extension is simple to implement and adds only a minor computational load, making it effectively as fast as the A* algorithm. However, Θ* solves the issue of a limited path directions by not restricting the path to adjacent nodes. The path is thus allowed to "jump" to the next appropriate node, even if it is not adjacent, to build a smooth path. It should be noted that, similar to the A*, Θ* is not guaranteed to find the truly shortest path [11].

The only difference between the code of A* and Θ* is in the `UpdateVertex` procedure seen in algorithm 1. The updated version can be seen in algorithm 2. The

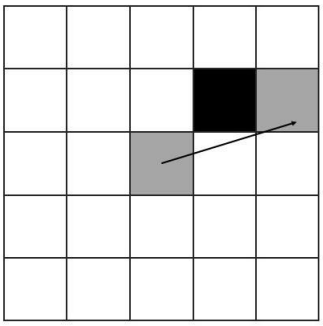

Figure 3.6: The Θ* search algorithm manage any angle path finding by not restricting the path to traverse only adjacent nodes.

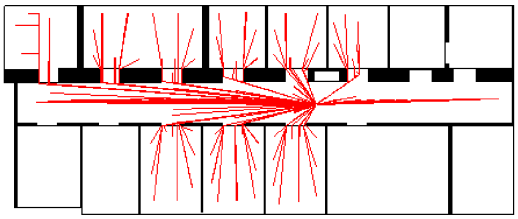

Figure 3.7: The Θ* search algorithm used to find dominant paths.

main changes in the UpdateVertex procedure is the new method `LineOfSight`. This method evaluates if two nodes are visible to each other, i.e., if there are obstacles in the way of a straight line between them. If the procedure evaluates to true, the shortest path between them is simply the straight line and Θ* will record a "jump" between the nodes as part of the path. If it is evaluated as false, then the algorithm must continue to search for a path around the obstacle. The `LineOfSight` procedure is equivalent to determine which pixels to select when drawing a straight line in a raster display. An algorithm that does this is Bresenham's line-drawing algorithm. The algorithm can be implemented with only integer operations which makes it very fast.

The Θ* search algorithm was also implemented in Matlab and simulated in the same way as the A* search algorithm detailed in subsection 3.3.1. An example of the result can be seen in figure 3.7.

Algorithm 2 Θ* search algorithm

```
1:  procedure UpdateVertex
2:      if LineOfSight(parent(s), s') then
3:          if g(parent(s)) + c(parent(s), s') < g(s') then
4:              g(s') := g(parent(s)) + c(parent(s), s')
5:              parent(s') := parent(s)
6:              if s' ∈ open then
7:                  open.Remove(s')
                open.Insert(s', g(s') + h(s'))
8:      else
9:          if g(s) + c(s, s') < g(s') then
10:             g(s') := g(s) + c(s, s')
11:             parent(s') := s
12:             if s' ∈ open then
13:                 open.remove(s')
14:             open.Insert(s', g(s') + h(s'))
```

3.5 Source code

The source code for the Matlab implementation of the A*/Θ* search algorithms is available on Github at `https://github.com/Thoronion/Astar-Thetastar-MATLAB`.

Chapter 4

Propagation model evaluation

In chapter 2, four propagation models for indoor environments were introduced. In chapter 3, algorithms to implement the models were described. In this chapter, all the models are tested and evaluated at three different test sites and the results are presented.

4.1 Experimental set-up

4.1.1 Test sites

To evaluate the radio propagation models detailed in chapter 2, a few test sites were required. Three different floors with various characteristics were chosen in two separate buildings.

GH - Greenhouse

The first test site (GH) was the entrance floor of a ten story apartment building called Greenhouse, located in Malmö, Sweden. GH is constructed to be as energy efficient as possible, with windows and isolation specialized to keep the heat energy within the building. Consequently, radio signals will experience difficulties penetrating the walls and the radio coverage inside the building is poor. As a counter measure, a repeater has been installed in the basement which receives signals from an antenna mounted on the roof top and redistributes the signal to indoor antennas mounted in the stairway on every floor. However, the antennas in the stairway do not guarantee sufficient coverage in the apartments and common areas. As access to the apartments was highly restricted, the entrance floor was used as a surrogate. The binary representation of the floor can be seen in figure 4.1.

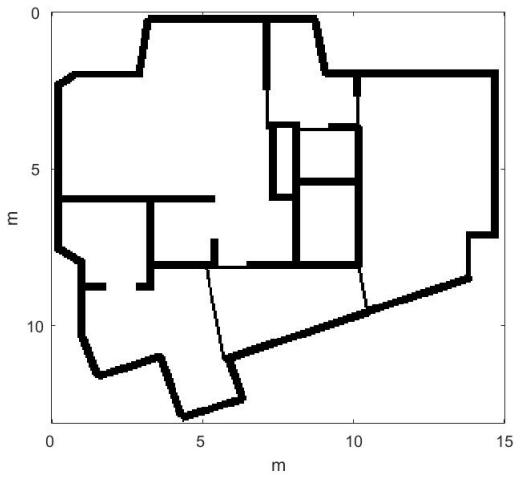

Figure 4.1: A binary image map over the test site Greenhouse.

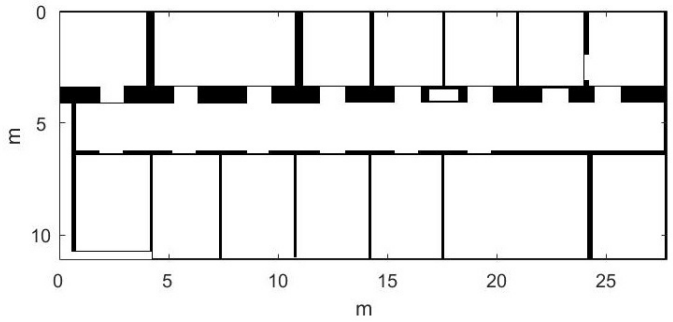

Figure 4.2: A binary image map over the office corridor in the Centre for Mathematical Sciences which was used as a test site.

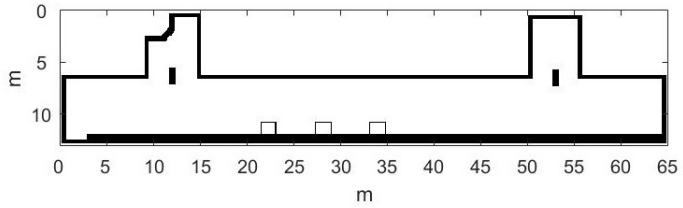

Figure 4.3: A binary image map over the foyer in the Centre for Mathematical Sciences which was used as a test site.

MH1 - Office corridor in the Centre for Mathematical Science

The second test site (MH1) was an unoccupied office floor in the building of the Centre for Mathematical Sciences at Lund University in Lund, Sweden. A main corridor of 27 meters runs across the entire floor. The corridor is further flanked by adjacent offices and storage rooms as seen in figure 4.2. Since the corridor was unoccupied, it was easy to gain access to the offices to conduct measurements without disturbing daily work. To minimize the prediction area and speed up the calculations, the measurements were restricted to the offices and the corridor. This was justifiable as storage areas are visited sporadically and generally for shorter periods, and are thus generally not prioritized during network planning.

MH2 - Foyer in the Centre for Mathematical Science

The third, and last, test site (MH2) was the foyer at the Centre for Mathematical Sciences, as shown in figure 4.3. It is approximately 65 meters long and 7 meter wide. It consists mainly of an open area, except for two pillars located on either side of the foyer. The walls and the pillars are made of bricks. This test site was selected to represent a large open area, such as a shopping mall or a metro station.

4.1.2 Equipment and Measurement

To measure the received signal strength, a Sony Z3 smart phone was used. The smart phone is a simple hand-held device which makes it easy to use and carry around. The use of smart phones for making calls and using data communication services indoors is widespread, thus making the smart phone a suitable test device for this project.

The measurements of the received signal strength were collected by walking around the corridor area with the smart phone. The sampling of the signal strength was carried out automatically using an application called TEMS Pocket, which was installed on the smart phone. Since the GPS-coverage indoors is strictly limited and rather inaccurate, manual pinpointing was used to register the walking path. Consequently, measurements collected lack information about location and only contains time stamp and received signal strength value. Thus, the measurements must be manually interpolated. For instance, consider a measuring session that ends up with N waypoints that were manually pinpointed, called $\mathbf{w}_1$, $\mathbf{w}_2$, ..., $\mathbf{w}_N$, respectively. These waypoints were pinpointed at times $T_1, T_2, \ldots, T_N$, which are the times elapsed since the session started. Thus, the i:th measurement, provided by the smart phone, has time stamp t_i and its location $\mathbf{p}_i$ is to be determined. This was performed by finding indices L and U such that

$$t_i \in [T_L, T_U] \tag{4.1}$$

is fulfilled. For the interpolation to work, the time, t_i, must be normalized on the interval (4.1) as

$$\hat{t}_i = \frac{t_i - T_L}{T_U - T_L}. \tag{4.2}$$

After that, the linear interpolation between corresponding way points $\mathbf{w}_L$ and $\mathbf{w}_U$ is performed as

$$\mathbf{p}_i = \begin{pmatrix} 1 & \hat{t}_i \end{pmatrix} \begin{pmatrix} 1 & 0 \\ -1 & 1 \end{pmatrix} \begin{pmatrix} \mathbf{w}_L \\ \mathbf{w}_U \end{pmatrix}. \tag{4.3}$$

To handle the interpolation, a program was written in C# to handle the conversion between the formats. A Matlab script was further created to import the data and interpolate the measurements between the extracted way points.

4.1.3 Parameter estimation

The propagation models presented in chapter 2 are formulated as

$$P_r(d) = P_{r|d_0} + 10\gamma \log_{10}(d) \tag{4.4}$$

where $P_{r|d_0}$ and γ are treated as unknown parameters. Therefore, these parameters need to be estimated from measurement data. A simple and effective method for estimating these parameters is the ordinary least square method. Ordinary least squares selects the parameters that minimizes the squared sum over the model residuals. Let d_i denote the Euclidean distance between the transmitter location $\mathbf{x}$ and the i:th measurement location $\mathbf{p}_i$, i.e.,

$$d_i = ||\mathbf{x} - \mathbf{p}_i||_2. \tag{4.5}$$

The relationship between the received signal strength in location i, denoted r_i, and the distance d_i can be expressed as

$$r_i = \mathbf{x}_i^T \boldsymbol{\beta} + \varepsilon_i \tag{4.6}$$

where

$$\mathbf{x}_i = \begin{pmatrix} 1 \\ 10\log_{10}(d_i) \end{pmatrix}, \quad \boldsymbol{\beta} = \begin{pmatrix} P_{r|d_0} \\ \gamma \end{pmatrix} \tag{4.7}$$

with ε_i denoting the error between the measured signal strength and the predicted value, i.e.,

$$\varepsilon_i = r_i - \mathbf{x}_i^T \boldsymbol{\beta}. \tag{4.8}$$

The relationship in (4.6) can be expressed more compactly as

$$\mathbf{r} = \mathbf{X}\boldsymbol{\beta} + \boldsymbol{\varepsilon} \tag{4.9}$$

where

$$\mathbf{r} = \begin{pmatrix} r_1 \\ r_2 \\ \vdots \\ r_N \end{pmatrix}, \quad \mathbf{X} = \begin{pmatrix} \mathbf{x}_1^T \\ \mathbf{x}_2^T \\ \vdots \\ \mathbf{x}_N^T \end{pmatrix} \quad \text{and} \quad \boldsymbol{\varepsilon} = \begin{pmatrix} \varepsilon_1 \\ \varepsilon_2 \\ \vdots \\ \varepsilon_N \end{pmatrix}, \tag{4.10}$$

assuming there are N data samples. The sum of the squared residuals is used as a measure of how well the model fits the data. Thus, the estimated parameters are the ones that minimize the sum, i.e.,

$$\hat{\boldsymbol{\beta}} = \arg\min_{\boldsymbol{\beta}} ||\mathbf{r} - \mathbf{X}\boldsymbol{\beta}||_2^2 \tag{4.11}$$

where $\hat{\boldsymbol{\beta}}$ is the optimal solution to the optimization problem. The solution to the ordinary least square problem is well known [16] and may be expressed in matrix form as

$$\hat{\boldsymbol{\beta}} = \left(\mathbf{X}^T\mathbf{X}\right)^{-1}\mathbf{X}^T\mathbf{r}. \tag{4.12}$$

The estimated parameters $\hat{\boldsymbol{\beta}}$ are then used to form the predictor

$$\hat{\mathbf{r}} = \mathbf{X}\hat{\boldsymbol{\beta}}. \tag{4.13}$$

4.1.4 Normal distribution fitting

To get an idea of the accuracy of the predictions, the estimated residuals

$$\hat{\boldsymbol{\varepsilon}} = \mathbf{r} - \hat{\mathbf{r}} \tag{4.14}$$

are formed. As stated in section 2.4.1, the residuals of the models may be expected to fit the normal distribution which has the probability density function

$$\phi(x) = \frac{1}{\sqrt{2\sigma^2\pi}} e^{-\frac{(x-\mu)^2}{2\sigma^2}} \tag{4.15}$$

where μ is the mean and σ the standard deviation of the distribution. These parameters are unknown and need to be estimated. The estimated mean, $\hat{\mu}$, and the variance, $\hat{\sigma}^2$, are estimated according to

$$\hat{\mu} = \frac{1}{N}\mathbb{1}_N^T\hat{\boldsymbol{\varepsilon}} \quad \text{and} \quad \hat{\sigma}^2 = \frac{1}{N-1}||\hat{\boldsymbol{\varepsilon}} - \hat{\mu}\mathbb{1}_N||_2^2. \tag{4.16}$$

where

$$\mathbb{1}_N = \left.\begin{pmatrix} 1 \\ 1 \\ \vdots \\ 1 \end{pmatrix}\right\} N \text{ ones.} \tag{4.17}$$

The cumulative distribution function of the fitted normal distribution is then

$$\Phi(x) = \int_{-\infty}^{x} \phi(t)\, dt \tag{4.18}$$

which compared to the empirical distribution function is calculated as

$$\hat{\Phi}(x) = \frac{1}{N}\sum_{i=1}^{N} \mathbf{1}_{r_i \leq x} \tag{4.19}$$

where

$$\mathbf{1}_{r_i \leq x} = |\{i : r_i \leq x\}|. \tag{4.20}$$

The indicator function $\mathbf{1}_{r_i \leq x}$ indicates how many population samples r_i that are less than or equal to x.

Table 4.1: Comparison between propagation models evaluated at Greenhouse.

model	**mean error**	**std. deviation**
one-slope	8.20	9.93
dual-slope	4.45	5.71
dominant path, A*	6.52	8.04
dominant path, Θ*	6.30	7.74
dual-slope dominant path, A*	3.63	4.49
dual-slope dominant path, Θ*	3.73	4.67

4.2 Evaluation of models

The test site GH was utilized to evaluate the radio propagation models in chapter 2. In this scenario, an access point was placed at GH, as shown in figure 2.1a. This placement corresponds to the real positioning of access points in the building. The intention of this placement was that it would hopefully provide coverage throughout the floor. However, as seen in the figure, an elevator shaft is located between the access point and the lower part of the rightmost room. If a device is placed there will it experience enough coverage from the transmitter?

In order to determine this measurement data were collected at the test site. Then, model parameters were estimated to make predictions. The predictions were then compared to the measurements to get an idea about the models under ideal condition when plenty of measurement data is available.

4.2.1 Summary of the results

All the models were evaluated at GH. The mean error and the estimated standard deviation for every model have been summarized in table 4.1. As can be seen, the one-slope model does have problems with accuracy, as expected. Furthermore, the dominant path model shows an improvement compared to the one-slope model. There was also a slight difference between using the A*, as shown in figure 4.8a, or Θ*, shown in figure 4.8b. The Θ* algorithm showed a slightly better result, except for the dual-slope dominant path model that showed the opposite. The dual-slope extension of both models enhanced the prediction accuracy considerably.

The estimated parameters for all the evaluated models at GH have been summarized in table 4.2. The reference parameter $P_{r|d_0}$ varies between -38 and -27 dBm and the path loss exponents varies in the range 3.1 to 3.9, which was expected according to the exemplary values in table 2.1. In the LOS environment, the path loss exponent is below the free space value of 2, which also corresponded to the expectations since there are no obstacles in its way and due to wave guiding, i.e., walls, floors, and ceiling will reflect signals that in free space would not reach the receiver.

Most of the residuals seemed to follow a normal distributed pattern. In figure 4.4a, a normal probability plot compared to the residual data is shown for the best performed model in GH, the dual-slope dominant path model. The cor-

Table 4.2: Estimated model parameters for all the evaluated propagation models at Greenhouse.

model	$\boldsymbol{\beta}_1$	$\boldsymbol{\beta}_2$	$\boldsymbol{\beta}_{\text{los}_1}$	$\boldsymbol{\beta}_{\text{los}_2}$	$\boldsymbol{\beta}_{\text{nlos}_1}$	$\boldsymbol{\beta}_{\text{nlos}_2}$
one-slope	-33.3	3.1	–	–	–	–
dual-slope	–	–	-35.8	0.6	-38.3	3.2
dominant path, A*	-27.2	3.7	–	–	–	–
dominant path, Θ*	-27.0	3.7	–	–	–	–
dual-slope dominant path, A*	–	–	-35.5	0.6	-29.2	3.9
dual-slope dominant path, Θ*	–	–	-35.5	0.6	-28.5	3.9

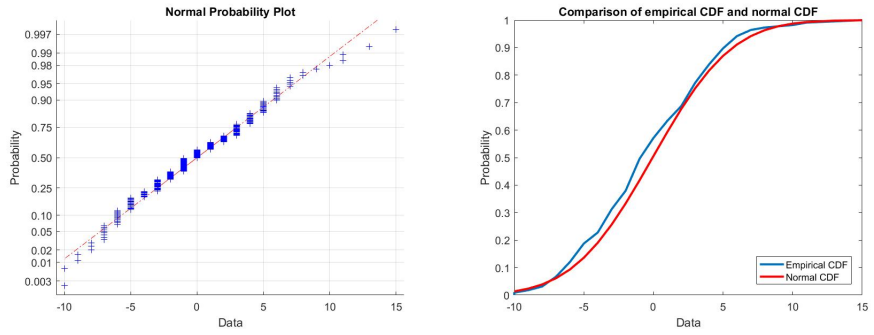

(a) (b)

Figure 4.4: In (a), normal probability plot for the residuals of the dual-slope dominant path model. In (b), the empirical cumulative distribution function (blue) of the residuals compared to the estimated cumulative distribution function (red).

responding empirical cumulative distribution function of the residuals together with the true cumulative distribution function of the fitted normal distribution is shown in figure 4.4b. The predictions made by the dual-slope dominant path model compared to the measurements along with residuals are displayed in figure 4.9.

4.2.2 LOS and NLOS classification

The dual-slope model and the dual-slope dominant path model require every sample to be classified as LOS or NLOS prior to the estimation of the model parameters. Since the floor is represented by a binary format, Bresenham's algorithm can easily be applied to determine LOS/NLOS relations. Figure 4.7 shows the result of the algorithm when deployed at GH. Blue samples indicate LOS condition and red samples are NLOS. As the figure shows, the algorithm is very accurate. The data was then separated in two sets and fitted to two different slopes. Figure 4.5b shows all the measurements collected at GH together with the LOS/NLOS-classification. The figure supports the idea that the accuracy can be enhanced by modelling LOS and NLOS separately.

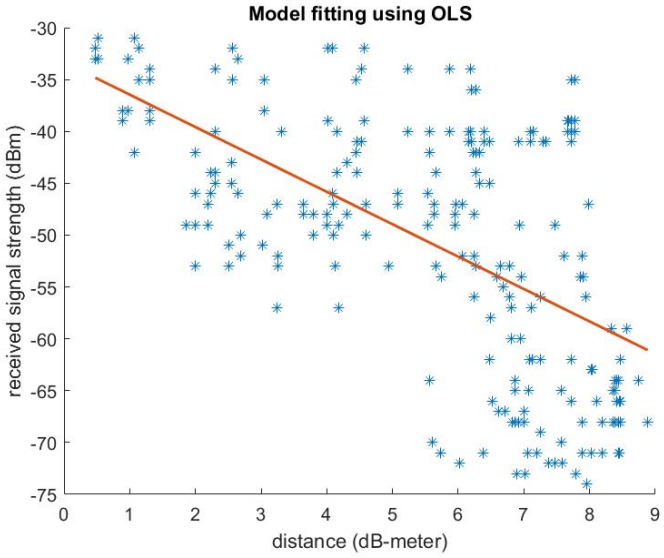

(a)

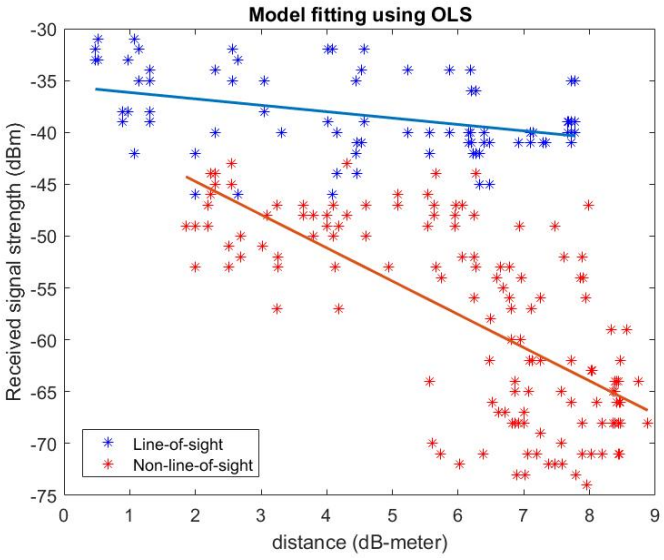

(b)

Figure 4.5: The one slope model fitted to measurement data in GH (a) compared to the dual-slope model fitted to the same data set (b).

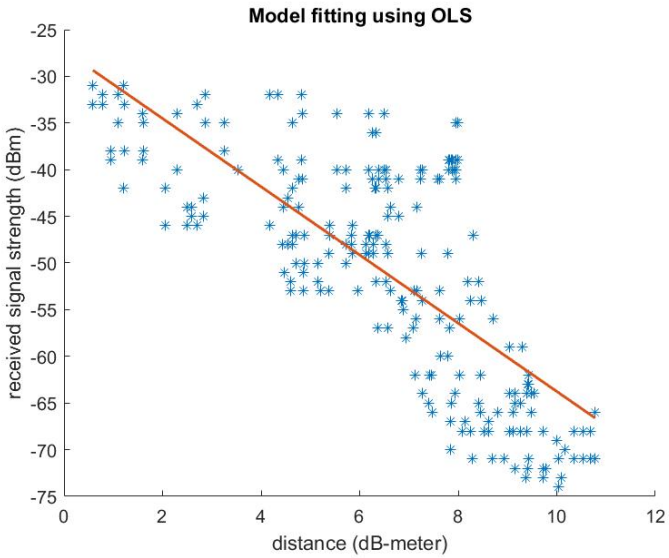

(a)

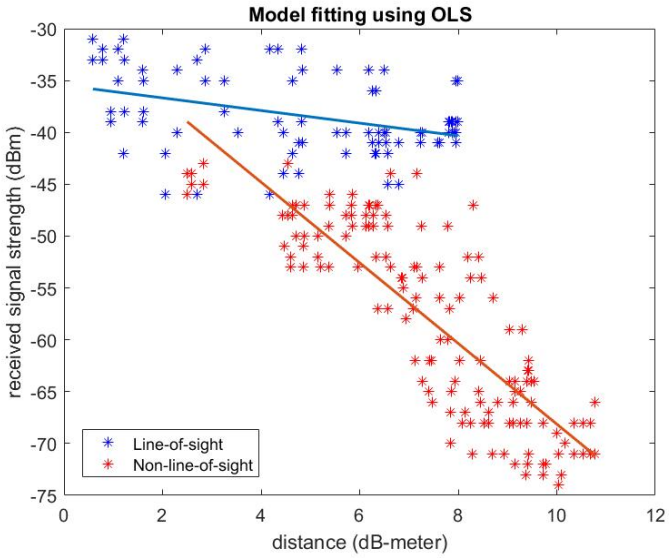

(b)

Figure 4.6: The dominant model fitted to measurement data in GH (a) compared to the dual-slope dominant path model fitted to the same data set (b). The A* search algorithm was used to retrieve the paths.

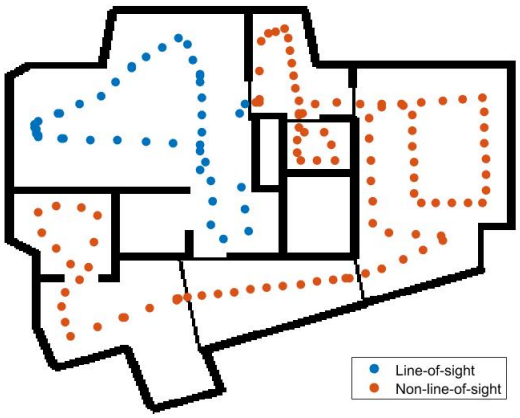

Figure 4.7: Bresenham's algorithm is used to determine if a sample is line-of-sight (blue) or non-line-of-sight (red) from the transmitter.

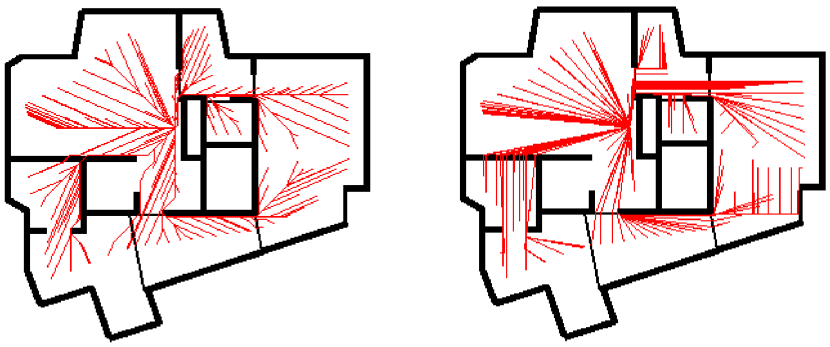

(a) (b)

Figure 4.8: Dominant paths found by the A* search algorithm (a), and the Θ* search algorithm (b), at GH.

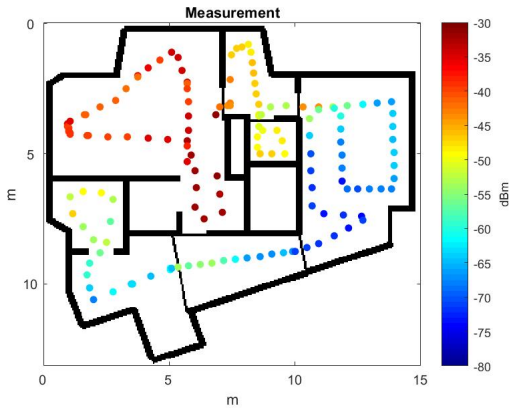

(a)

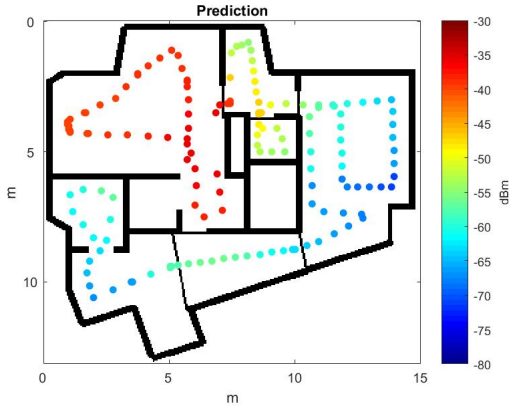

(b)

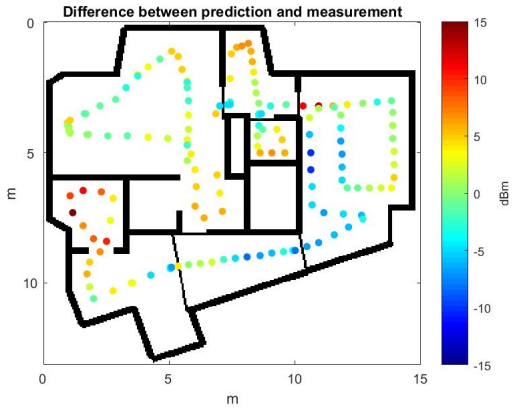

(c)

Figure 4.9: Predictions at GH using the dual-slope dominant path model. The paths were calculated using the A* search algorithm. Figure (a) depicts the measurements, (b) the predicted values, and (c) the difference between measurement and prediction.

Table 4.3: Comparison between models evaluated at test site MH1.

Model	Mean error	Std. deviation
one-slope	5.89	7.37
dual-slope	5.50	7.00
dominant path, A*	5.73	7.27
dominant path, Θ*	5.65	7.18
dual-slope dominant path, A*	5.50	7.00
dual-slope dominant path, Θ*	5.48	7.02

4.3 Comparison between sites

In the previous section, all the models were evaluated at GH. In conclusion, the dominant path models showed an improved prediction accuracy compared to their direct path counterparts when a high attenuating obstacle, such as an elevator shaft, is situated in a critical location. To strengthen the results of the evaluation, the models were evaluated by further applying them at the two remaining test sites, MH1 and MH2. The evaluation followed the same procedures as GH.

MH1

A comparison between the models evaluated at MH1 can be seen in table 4.3. Compared to GH, there are no apparent difference in the models performances. The mean error is around 5.7 dBm and the standard deviation around 7.2 dBm. This behaviour could perhaps be explained by looking at the dominant paths generated in the corridor by the A* and Θ* search algorithms, as shown in figures 3.5 and 3.7. Since there are no critical obstacles hindering the paths, the dominant paths are similar to the direct paths.

The estimated model parameters for MH1 has been summarized in table 4.4. Compared to GH, the reference parameters $P_{r|d_0}$ was in the range -46 to -42 dBm, which is a bit lower than at GH. An explanation could be that other types of access points were mounted in the corridor. The path loss exponents appear to be in the range 1.8 to 2.7, which is close to free space. This could indicate that the wave guiding effect in the corridor contributes to the relatively small path loss. Even the NLOS exponents are small, which would indicate that the walls do not attenuate the signal heavily.

The model that performed the best, considering result, speed, and implementation, was the dual-slope model. The slopes fitted to the data can be seen in figure 4.10. It is clear that there is no big difference between the LOS and NLOS conditions. The normality plots for the model can be seen in figure 4.11. Except for some outliers, the residuals appear to fit a normal distribution. The predictions compared to measurements as well as residuals are plotted in figure 4.12. All plots corresponding to the remaining model evaluations can be found in the appendix.

Table 4.4: Estimated model parameters for all the propagation models evaluated at test site MH1.

model	$\boldsymbol{\beta}_1$	$\boldsymbol{\beta}_2$	$\boldsymbol{\beta}_{\text{los}_1}$	$\boldsymbol{\beta}_{\text{los}_2}$	$\boldsymbol{\beta}_{\text{nlos}_1}$	$\boldsymbol{\beta}_{\text{nlos}_2}$
one-slope	-45.4	2.3	–	–	–	–
dual-slope	–	–	-45.7	1.8	-42.3	2.7
dominant path, A*	-44.1	2.3	–	–	–	–
dominant path, Θ*	-44.6	2.3	–	–	–	–
dual-slope dominant path, A*	–	–	-45.7	1.8	-42.3	2.7
dual-slope dominant path, Θ*	–	–	-46.2	1.8	-42.8	2.6

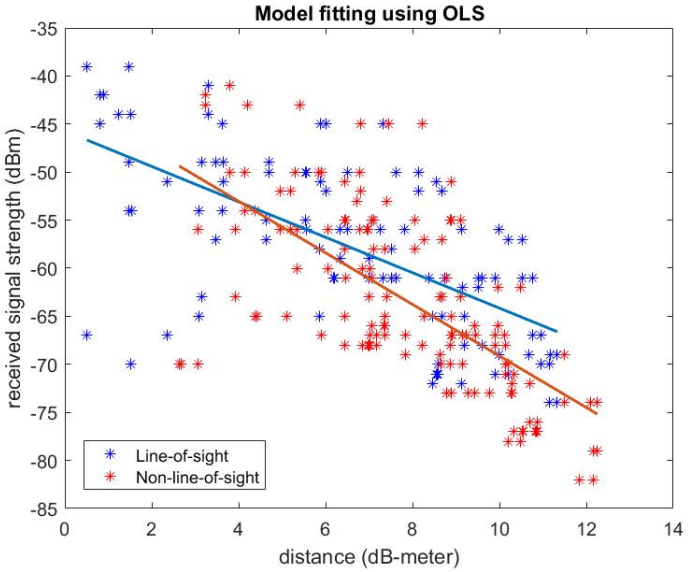

Figure 4.10: The dual-slope model fitted to measurement data from test site MH1 using ordinary least squares.

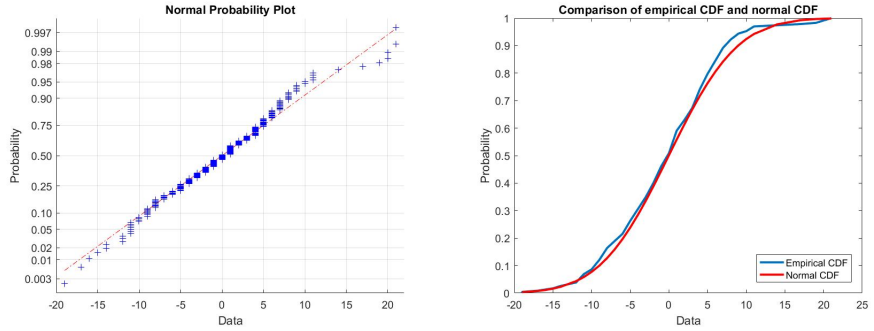

(a) (b)

Figure 4.11: In (a), normal probability plot for the residuals of the dual-slope model at test site MH1. In (b), the empirical cumulative distribution function (blue) of the residuals compared to the estimated cumulative distribution function (red).

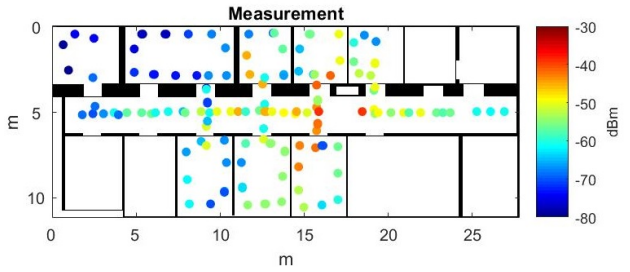

(a)

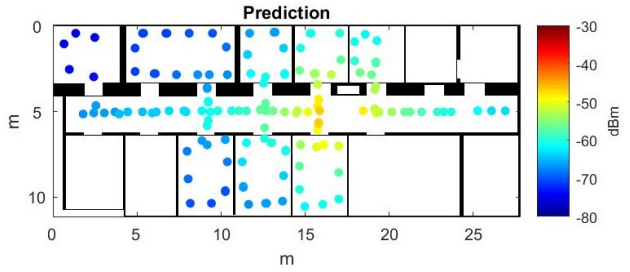

(b)

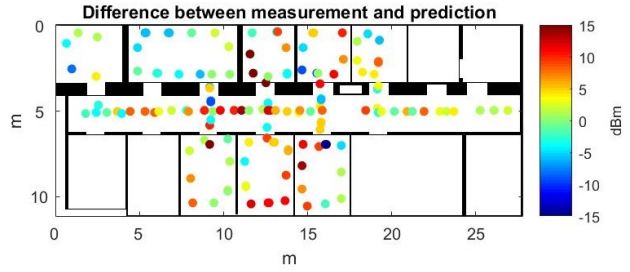

(c)

Figure 4.12: Predictions at MH1 using the dual-slope model. Figure (a) depicts the measurements, (b) the predicted values, and (c) the difference between measurement and prediction.

Table 4.5: Comparison between propagation models evaluated at MH2.

Model	**Mean error**	**Std. deviation**
one-slope	3.88	4.96
dual-slope	3.67	4.84
dominant path, A*	3.86	4.96
dominant path, Θ*	4.01	5.30
dual-slope dominant path, A*	3.67	4.84
dual-slope dominant path, Θ*	3.78	5.05

Table 4.6: Estimated model parameters for all the propagation models evaluated at MH2.

model	$\boldsymbol{\beta}_1$	$\boldsymbol{\beta}_2$	$\boldsymbol{\beta}_{\text{los}_1}$	$\boldsymbol{\beta}_{\text{los}_2}$	$\boldsymbol{\beta}_{\text{nlos}_1}$	$\boldsymbol{\beta}_{\text{nlos}_2}$
one-slope	-46.1	2.7	–	–	–	–
dual-slope	–	–	-45.0	2.7	-69.7	0.5
dominant path, A*	-45.6	2.7	–	–	–	–
dominant path, Θ*	-42.2	2.3	–	–	–	–
dual-slope dominant path, A*	–	–	-45.0	2.7	-69.7	0.5
dual-slope dominant path, Θ*	–	–	-42.0	2.3	-69.2	0.4

MH2

The last test site used for evaluation was MH2. The foyer is mainly an open without any obstructing obstacles. Thus, the majority of the area is considered LOS environment. The comparison between the propagation models has been summarized in table 4.5, where it can be seen that there are no big differences between the models. The model parameters are listed in table 4.6. The reference parameter are in the same range as the office corridor, which is to be expected as the same type of access point is used. The path loss exponents are very stable, probably due to the non-obstructive environment. However, the NLOS parameters are significantly different as compared to the LOS. Since most of the area was considered LOS environment and a significant amount of NLOS measurement were missing, the parameters should not be trusted.

The dual-slope model fitted to the measurement data can be seen in figure 4.13. The normality plots is shown in figure 4.14 and, as can be seen from the figure, the residuals do not appear to be normally distributed. The comparison between predictions and measurement along with residuals can be seen in figure 4.15. All other plots corresponding to the evaluation of the remaining models at MH2 can be found in the appendix.

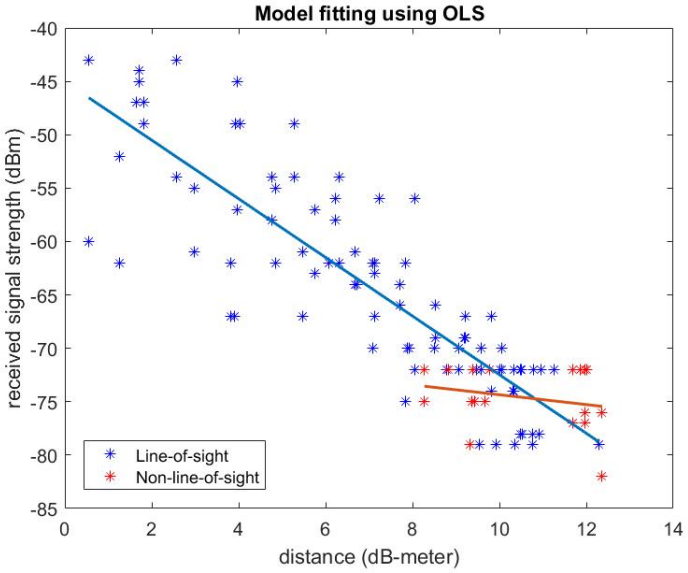

Figure 4.13: The dual-slope model fitted to measurement data at MH2 using ordinary least squares.

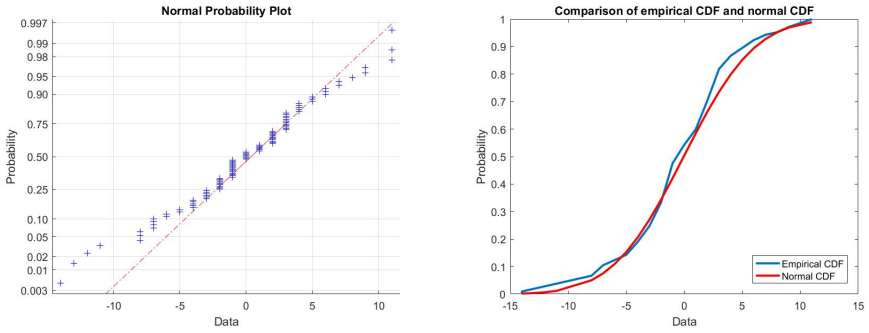

(a) (b)

Figure 4.14: In (a), normal probability plot for the residuals of the dual-slope model at test site MH2. In (b), the empirical cumulative distribution function (blue) of the residuals compared to the estimated cumulative distribution function (red).

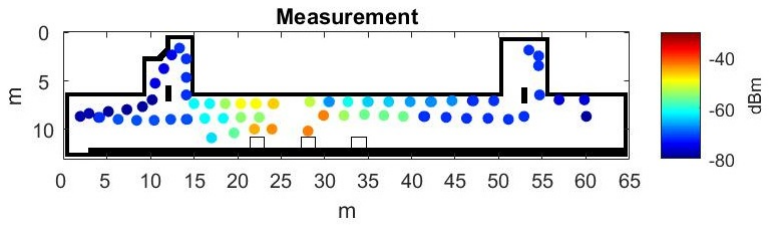

(a)

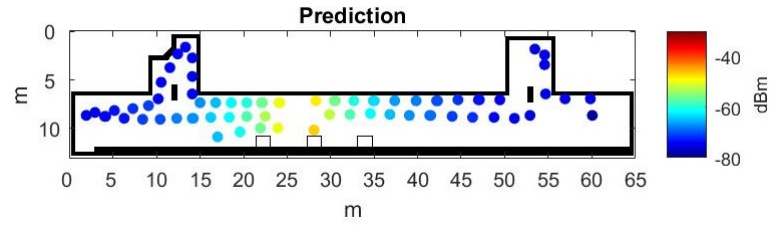

(b)

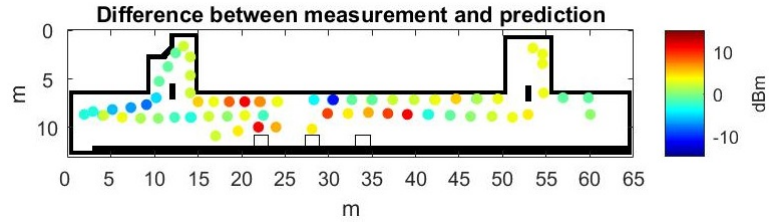

(c)

Figure 4.15: Predictions at MH2 using the dual-slope model. Figure (a) depicts the measurements, (b) the predicted values, and (c) the difference between measurement and prediction.

Chapter 5

Antenna placement

In the previous chapter, the propagations models were evaluated at different test sites. The evaluation showed that some of them have potential to produce fairly accurate predictions given well estimated parameters. In this chapter, the problem of choosing the best subset of antennas that guarantees a certain coverage, given suitable antenna locations, is studied.

5.1 Coverage decision

Radio planning in indoor environments can be challenging. It is difficult to predict the coverage based on the location of the antennas. However, as pointed out in chapter 1, it is not often necessary to know the exact coverage at a specific location. Instead, it can be sufficient to know if the coverage will most likely be over a certain threshold. From our previous discussions, it has been seen that the residuals for some of the models followed a pattern corresponding to the normal distribution. This information is very useful for the accuracy of the predictions. For instance, assume that in one location i, it is desired that the coverage will exceed a threshold t_i. Since the residuals are normal distributed, it follows that

$$r_i \sim N(\mathbf{x}_i^T \boldsymbol{\beta}, \sigma^2) \tag{5.1}$$

where σ is the standard deviation of the residuals. Let the estimated variance of the residuals be denoted s^2, then the estimated expected value of the received signal strength, given the log-distance vector $\mathbf{x}_i$, may be expressed as

$$\hat{E}(r_i|\mathbf{x}_i) = \mathbf{x}_i^T \hat{\boldsymbol{\beta}}, \tag{5.2}$$

where r_i is approximately distributed as

$$r_i \sim N(\mathbf{x}_i^T \hat{\boldsymbol{\beta}}, s^2). \tag{5.3}$$

Furthermore, assume that if a target is predicted to be over the threshold, it is necessary to be certain down to a probability p that the prediction is true, i.e.,

$$P(r_i > t_i|\mathbf{x}_i^T \hat{\boldsymbol{\beta}}) \geq p \quad \forall i. \tag{5.4}$$

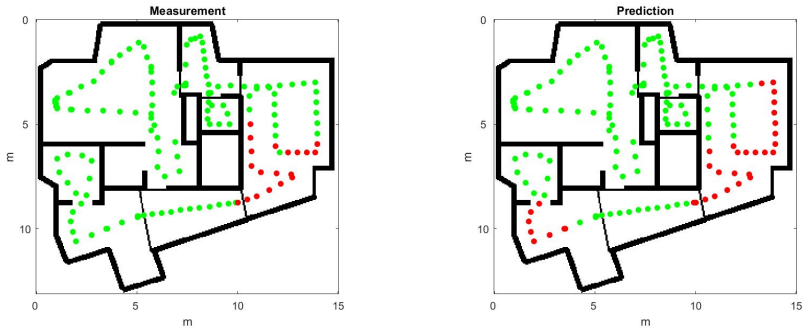

(a) (b)

Figure 5.1: Measurement and predictions in Greenhouse using the dual-slope dominant path model. Green samples are received signal strength values that are over −70 dBm. Red represents samples that are not. Figure (a) depicts the measured signal strength and (b) depicts predicted signal strength using a 95 percent marginal.

The inequality requires the prediction to be at least

$$\mathbf{x}_i^T \hat{\boldsymbol{\beta}} \geq t_i + s\sqrt{2}\,\mathrm{erf}^{-1}(2p-1) \tag{5.5}$$

to guarantee coverage over the threshold with $100p$ percent probability. Here, the function erf^{-1} is the inverse error function, defined as

$$\mathrm{erf}(x) \triangleq \frac{2}{\sqrt{\pi}} \int_0^x e^{-t^2}\, dt. \tag{5.6}$$

To demonstrate the concept, lets go back to the entrance floor at GH, recalling the scenario described in section 4.2. One access point was placed at the test site with the assumption that it would provide coverage in all areas. Assume that the threshold for coverage has been set to −70 dBm, i.e.,

$$t_i = -70 \quad \forall i. \tag{5.7}$$

Furthermore, assume that the model used for prediction is the dual-slope dominant path model using the modified A* search algorithm for finding the dominant paths, where the model parameters given in table 4.2. The estimated standard deviation of the residuals was then

$$s = 4.49. \tag{5.8}$$

If p is set to 0.95, then the minimum predicted value, r_{lim}, that with at least 95 percent probability will be over the threshold will be

$$r_{\mathrm{lim}} \approx -63. \tag{5.9}$$

Figure 5.1 shows the comparison between measurements and predictions. The locations that according to the measurements have a coverage over −70 dBm is shown in (a) with green color while the locations that do not are red. It can

be seen from the measurements that the coverage will not be sufficient in the room to the far right probably due to the elevator shaft in between the access point and the targets. In (b), the decisions based on the predictions are shown. Green locations indicate that it is 95 percent certain that the coverage is over -70 dBm and red indicate that the coverage might or might not be over the threshold. It is clear that the model also draws the conclusion that the coverage is not sufficient in the room to the far right.

5.2 Problem formulation

In the previous section, it was concluded that one access point was not enough to provide good coverage in all areas at GH. Since this was a requirement, the question arises where to place additional access points - or will one be enough if at another location? It is often desired to minimize the number of antennas. Few antennas means less hardware and cables, which will reduce the cost for equipment as well as installation work. Physical space is also an important parameter since the potential locations to mount antennas might be restricted to were the wall sockets are located, and/or aesthetic conditions.

Antenna selection is closely related to sensor selection in a network [5]. The antenna selection problem can be formulated as an optimization problem. Let N be the number of target locations, with t_i denoting the desired minimum coverage at a specific target location $i \in \Omega = \{1, 2, \ldots, N\}$. Furthermore, let M be the number of possible antenna locations where j refers to a specific antenna. Then, an $M \times N$ prediction matrix can be constructed as

$$\hat{\mathbf{R}} = \begin{pmatrix} \hat{r}_{11} & \hat{r}_{12} & \cdots & \hat{r}_{1N} \\ \hat{r}_{21} & \hat{r}_{22} & \cdots & \hat{r}_{2N} \\ \vdots & \vdots & \ddots & \vdots \\ \hat{r}_{M1} & \hat{r}_{M2} & \cdots & \hat{r}_{MN} \end{pmatrix} \tag{5.10}$$

where $\hat{r}_{ji}$ denotes the predicted value at target location i from antenna j. Furthermore, let $\mathbf{e}_i$ denote a $N \times 1$ vector with all components set to zero, except one at place i, which is set to one. Then, $\hat{\mathbf{R}}\mathbf{e}_i$ will be a vector containing all the antenna contributions at target location i. Thus, the optimization problem can be formulated as follows

$$\mathbf{w}^* = \arg\min_{\mathbf{w}} ||\mathbf{w}||_0 \tag{5.11}$$

$$\text{s.t.} \quad ||\mathbf{w} \circ \hat{\mathbf{R}}\mathbf{e}_i||_\infty > t_i \quad \forall i \in \Omega \tag{5.12}$$

$$\mathbf{w} \in \{0, 1\}^M. \tag{5.13}$$

where $\mathbf{w}$ is an antenna selection vector with components w_j indicating whether an antenna j is selected (1) or not (0). Here, the ℓ_0-(quasi)norm is defined as the number of non-zero elements in a vector, i.e.,

$$||\mathbf{w}||_0 \triangleq |\{j : w_j \neq 0\}|. \tag{5.14}$$

Thus, equation 5.11 expresses the desire to minimize the number of antennas. The point-wise vector multiplication, $\mathbf{w} \circ \hat{\mathbf{R}}\mathbf{e}_i$, results in a vector were the j:th

component represents the predicted coverage from antenna j at target i. The ℓ_∞-norm is defined as the maximum component in $\mathbf{w} \circ \hat{\mathbf{R}}\mathbf{e}_i$. If $\mathbf{x}$ is a vector of size n, then the ℓ_∞-norm is defined as

$$||\mathbf{x}||_\infty \triangleq \max(|x_1|, |x_2|, \ldots, |x_n|). \tag{5.15}$$

The maximum norm in (5.12) simply extracts the strongest antenna contribution at every target location. Hence, it is a set of conditions that makes sure every target location gets sufficient coverage over the threshold t_i. Note that the formulation above requires the coverage to be expressed in linear scale, as it is necessary that $\hat{r}_{ji} > 0$, for all i and j.

The problem in 5.11 is combinatorial and involves finding a solution $\mathbf{w}^*$ that fulfils the conditions in 5.12 out of 2^M possible combinations of $\mathbf{w}$. The problem gets practically impossible to solve as M grows by iterating through every possible combinations. There can be many solutions that fulfils the optimization problem but since only one sufficient solution is needed this can be used to simplify the problem. The decision function δ decides whether a predicted value $\hat{r}_i$ is over the threshold t_i or not by assigning a one if it is over, and zero otherwise, i.e.,

$$\delta_{t_i}(\hat{r}_i) = \begin{cases} 1, & \hat{r}_i > t_i \\ 0, & \hat{r}_i \leq t_i. \end{cases} \tag{5.16}$$

A new matrix can then be constructed as

$$\hat{\mathbf{T}} = \begin{pmatrix} \delta_{t_1}(\hat{r}_{11}) & \delta_{t_2}(\hat{r}_{12}) & \cdots & \delta_{t_N}(\hat{r}_{1N}) \\ \delta_{t_1}(\hat{r}_{21}) & \delta_{t_2}(\hat{r}_{22}) & \cdots & \delta_{t_N}(\hat{r}_{2N}) \\ \vdots & \vdots & \ddots & \vdots \\ \delta_{t_1}(\hat{r}_{M1}) & \delta_{t_2}(\hat{r}_{M2}) & \cdots & \delta_{t_N}(\hat{r}_{MN}) \end{pmatrix} \tag{5.17}$$

where every element $\hat{\mathbf{T}}_{j,i}$ indicates if a target location i has coverage over the threshold t_i from antenna j. With the transformation, the optimization problem can be formulated as

$$\mathbf{w}^* = \arg\min_{\mathbf{w}} ||\mathbf{w}||_0 \tag{5.18}$$

$$\text{s.t.} \quad \hat{\mathbf{T}}^T\mathbf{w} \geq \mathbb{1}_N \tag{5.19}$$

$$\mathbf{w} \in \{0, 1\}^M. \tag{5.20}$$

5.3 Antenna selection algorithm

To solve the antenna selection problem in 5.18 only one feasible solution is required. The proposed algorithm to solve the problem is a greedy-search algorithm. The resulting algorithm is fast and easy to implement and finds a solution even if the number of targets and possible antenna location is large. The algorithm starts by summing the columns in $\hat{\mathbf{T}}$ and checks if any of the sums equals to one. This is the equivalent of checking if a target is only covered by one antenna and if that is the case the antenna must be selected. In the opposite case, when all targets can be covered by multiple antennas, the algorithm sums the rows in $\hat{\mathbf{T}}$. This is the equivalent of checking how many targets

Algorithm 3 Greedy search antenna selection algorithm

```
1: procedure OPTIMIZEANTENNAS
2:     i := 1
3:     w := 0_M
4:     V := ∅
5:     while T̂^(i) ≠ ∅ do
6:         s := 1_M^T T̂^(i)
7:         if s1_N = 0 then return No solutions exist
8:         if s_j = 1 for any j then
9:             find corresponding row in T̂^(i) and denote it k.
10:        else
11:            p := T̂^(i) 1_N
12:            find largest value in p and denote its position k.
13:            if a tie then
14:                select the row in R̂^(i) which maximize a predefined utility
                       function and denote that row k
15:        V.addLast(k)
16:        find all targets that antenna k covers and remove them from T̂^(i) and
               R̂^(i) thus creating T̂^(i+1) and R̂^(i+1)
17:        i := i +1
18:    for each k ∈ V do
19:        w_k := 1
       return w
```

a certain antenna covers. The antenna that covers most targets is selected. If there is a tie, then the antenna that maximizes a predefined utility function is chosen. This function can be adapted to fulfil different requirements. In either case, the antenna selected is removed from both the indicator matrix $\hat{\mathbf{T}}$ and the predicted coverage matrix $\hat{\mathbf{R}}$ and the algorithm starts over again with the new matrices. This continues until all targets are covered. The pseudo code of the algorithm can be found in algorithm 3.

5.4 Optimizing

To test the greedy search antenna selection algorithm, five possible locations to mount access points and six target locations where good coverage is important were selected at GH, as shown in figure 5.2.

To evaluate which antenna alternatives that fulfils the desired coverage, one access point was placed at one of the possible antenna locations and measurements were performed. Then, the access point was moved to next location and new measurements were taken. The same procedure was carried out using two access points that were varied over all possible combinations. Three or more access points were never evaluated since several alternatives with two access point were enough to provide coverage. The different antenna alternatives and their measurements can be seen in table 5.1.

In order to rank the antenna alternatives, the following utility function was

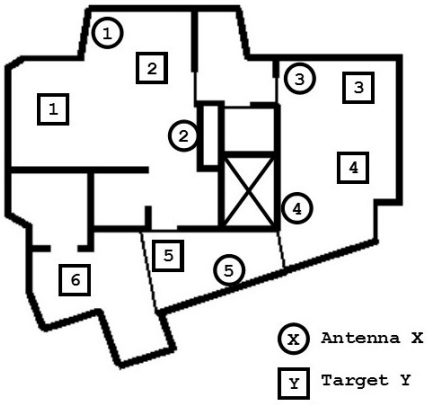

Figure 5.2: The greedy search antenna selection algorithm was tested at GH. Five possible antenna locations and six target locations were selected.

constructed

$$u_j = \prod_{i=1}^{N} \delta_{t_i}(r_i) \sum_{i=1}^{N} (r_i - t_i). \tag{5.21}$$

where u_j is the utility of antenna alternative j and N is the number of targets. The utility function sums the excess coverage over the threshold for every target, and if any target does not meet the threshold, the utility is set to zero. The different alternatives and their corresponding utility are plotted in figure 5.3. It can be seen that antenna alternative number 14 is the one that maximizes the utility function. However, the alternatives 6 through 8, as well as 11, are fulfilling the coverage requirement.

The dual dominant path with the modified A* search algorithm was used to predict the received signal strength on all targets, from all possible antenna locations. The result given in dBm was

$$\hat{\mathbf{R}}_{\text{dBm}} = \begin{pmatrix} -48 & -38 & -68 & -72 & -67 & -71 \\ -40 & -38 & -62 & -68 & -57 & -64 \\ -66 & -56 & -37 & -39 & -67 & -73 \\ -71 & -66 & -40 & -37 & -57 & -68 \\ -68 & -65 & -65 & -55 & -38 & -61 \end{pmatrix}. \tag{5.22}$$

The greedy search antenna selection algorithm was deployed upon the result with a desired threshold of -70 dBm and a requirement of 95 percent certainty that the suggested antenna combination will cover the targets. The algorithm suggested that antenna 2 combined with antenna 5 would be sufficient to provide coverage on all targets. The alternative corresponds to alternative 7 in table 5.1 and is marked with red in the utility plot in figure 5.3. This alternative does clearly meet the desired requirement of -70 dBm. Also note that according to the predictions in 5.22, antenna 2 and 5 would alone, independently of each other, not provide sufficient coverage on all targets. Hence, the extra marginal provided by the 95 percent certainty requirement is important to reduce the risk of over-minimizing the antennas.

Table 5.1: Different antenna alternatives and their corresponding measured received signal strength in six different target locations at GH.

Index	Antennas	$\mathbf{p}_1$	$\mathbf{p}_2$	$\mathbf{p}_3$	$\mathbf{p}_4$	$\mathbf{p}_5$	$\mathbf{p}_6$
1	1	-44	-40	-66	-73	-70	-62
2	2	-44	-38	-63	-74	-56	-68
3	3	-64	-58	-40	-43	-71	-78
4	4	-74	-69	-45	-42	-67	-78
5	5	-72	-70	-70	-61	-45	-53
6	1 & 5	-45	-43	-60	-60	-40	-52
7	2 & 5	-46	-40	-65	-57	-40	-55
8	3 & 5	-63	-55	-40	-49	-37	-62
9	4 & 5	-77	-74	-43	-40	-40	-57
10	3 & 4	-62	-53	-40	-40	-63	-70
11	2 & 4	-46	-40	-50	-39	-57	-61
12	1 & 4	-49	-41	-47	-47	-65	-66
13	1 & 3	-49	-39	-44	-49	-68	-67
14	2 & 3	-41	-46	-43	-40	-56	-60
15	1 & 2	-43	-38	-57	-69	-65	-64

In the scenario above, the model parameters were estimated using ordinary least squares out of a total of 224 measurement samples collected all over the test site. Out of these, 85 were collected in LOS from the transmitter and 139 were collected NLOS. This was enough to select an antenna alternative that fulfilled the coverage requirements, but what if less samples were available? Would the prediction model still be sufficiently good to determine a descent alternative? In the ideal case, it is not desired to conduct a full measurement survey on all areas prior to running the optimization. It would be desirable to spend as little time as possible on measuring to estimate the parameters.

Since the residuals were assumed to be normal distributed, it follows that the estimate of the model parameters, $\hat{\boldsymbol{\beta}}$, are also normal distributed, with expected value [16]

$$E(\hat{\boldsymbol{\beta}}) = \boldsymbol{\beta} \tag{5.23}$$

and variance

$$\mathrm{Var}(\hat{\boldsymbol{\beta}}) = \sigma^2(\mathbf{X}^T\mathbf{X})^{-1}. \tag{5.24}$$

If $\hat{\boldsymbol{\beta}}_{\mathrm{nlos}}$ are the estimated parameters for the NLOS part of the model used to predict 5.22 and s is the estimated standard deviation of the residuals, then the estimate is approximately distributed as [16]

$$\hat{\boldsymbol{\beta}} \sim N(\hat{\boldsymbol{\beta}}_{\mathrm{nlos}},\, s^2(\mathbf{X}^T\mathbf{X})^{-1}). \tag{5.25}$$

Assuming that the parameters for the LOS scenario are known and the parameters for NLOS are unknown; how likely is it that the optimization algorithm yields a solution containing the optimal number of antennas and an antenna alternative that gives the required coverage, given n NLOS samples to estimate the model parameters? This was simulated as follows,

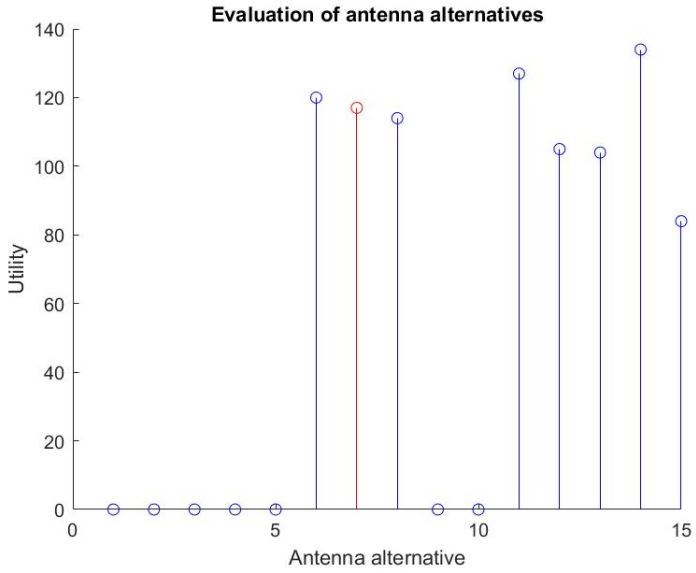

Figure 5.3: The utilities for the antenna alternatives in table 5.1. The red alternative is the one selected by the greedy search antenna algorithm using the dual-slope dominant path model for predictions.

1. Set n to 2.
2. Draw n samples uniformly at random from the NLOS locations of $\mathbf{X}$.
3. Draw 10000 estimated parameters from equation 5.25.
4. Calculate $\hat{\mathbf{R}}$ and run the antenna optimization algorithm for every parameter drawn in 3.
5. Save the number of times the algorithm succeeds selecting one of the optimal solutions.
6. Increment n by one and repeat the steps from 2.

The simulation was done with samples ranging from $n = 2$ to 139. This was summarized in figure 5.4, which shows the likelihood that the optimization algorithm selects one of the antenna alternatives containing the optimal number of antennas that sufficiently fulfils the coverage requirements. In (a) the reference parameter, $P_{r_2|d_0}$, has been treated as known while in (b) it is unknown. It can be seen that the optimization algorithm is approximately 90 percent likely to select an optimal solution at GH if the whole test site is sampled and the reference parameter is known and approximately 80 percent if the parameter is unknown. The same probabilities are approximately 75 and 65 percent if the number of samples available are reduced by half.

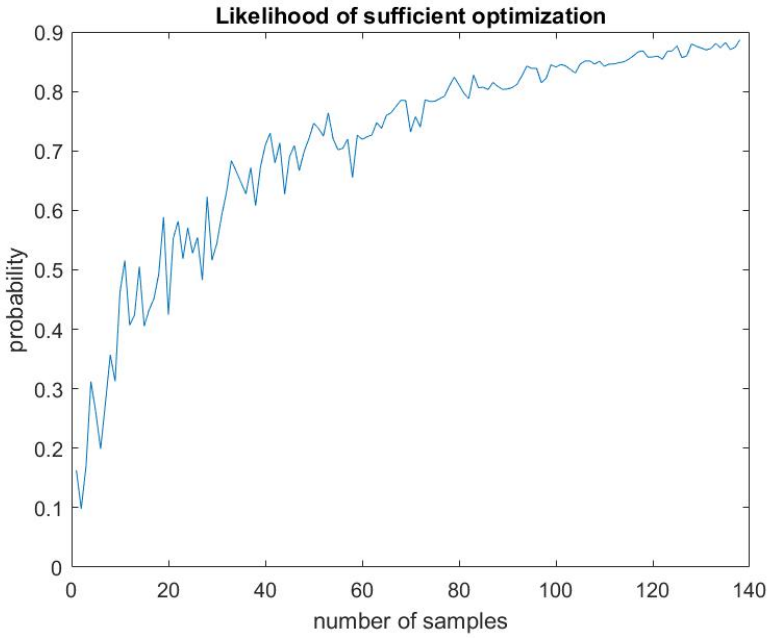

(a)

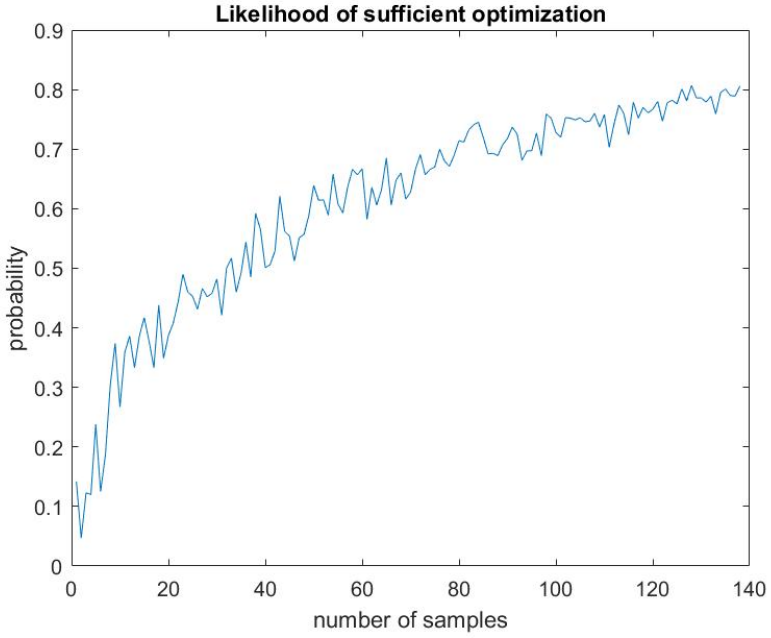

(b)

Figure 5.4: The likelihood that the optimization algorithm selects an antenna alternative containing the optimal number of antennas that sufficiently fulfils the coverage requirements given n samples to estimate the model parameters. In (a), the reference parameter $P_{r_2|d_0}$ is known and in (b) it is unknown.

Chapter 6

Conclusions and Discussion

6.1 Summary

In this master's thesis, several indoor radio propagation models have been studied. They have been tested and evaluated at three different test sites. The first test site, GH, was a compact area that contained several obstacles. The main obstacle was an elevator shaft situated in the centre of the floor that effectively blocked the radio signals. Greenhouse represented a residential scenario. The second test site, MH1, was a long corridor flanked by adjacent offices. The wall material was homogeneous and the floor outline was symmetrically designed. This test site represented an office scenario. The third, and last, test site, MH2, was a 65 meter long foyer in the same building as the previous test site. It represented a scenario with large open areas, e.g. a shopping mall or metro station.

In GH, the dominant path models significantly improved the predictions compared to their direct path counterparts. The elevator shaft is the most probable explanation to this as it will block the signals from the transmitter. The dominant path model, with path finding algorithms, could find paths around the shaft in contrast to the one-slope and the dual-slopes models that assumes a straight path through the shaft. Thus, the dominant path model will give a better representation at GH than the other two.

At MH1, there were no obstacles, except for the walls, that attenuate the signals. Interestingly, the difference between the prediction quality of the dominant and direct path model was insignificant. The most likely explanation to this is the lack of obstacles, e.g., the elevator shaft at GH. As MH1 and MH2 display rather similar characteristics, i.e., no major obstacles, it is not surprising that they also showed similar results, i.e., no significant difference between the models was identified.

To find the dominant paths, two path finding algorithms were used, namely the A* and Θ* search algorithms. The latter was introduced as an extension of the A* algorithm aiming to improve the paths by allowing them to expand in any angle, compared to the A* that can only expand in eight directions. This

would allow the path to constitute a better representation of the true distance of the path. However, no significant difference related to the search algorithms was identified. In conclusion, the distances between the paths found by the two search algorithms is probably insignificant.

The model parameters where estimated using ordinary least squares of measurements from the area of interest. The standard deviation of the predictions ranged between 4 and 10 dBm, depending on model and test site. For most of the models, the residuals appeared to follow a normal or an approximately normal distribution pattern. This is an important observation since it it is helpful when making conclusions about the certainty in a prediction. Since the thesis deal with empirical or semi-deterministic indoor propagation models it is not surprising that the standard deviation is relatively high. This is a well known fact. However, the purpose of this master's thesis was to investigate if the prediction could be useful to make general conclusions about the coverage, i.e., if the received signal strength exceeds a desired threshold or not, and be utilized for optimization purposes.

GH was further utilized for the optimization part of the thesis. There were five possible antenna locations and six target areas, i.e., areas where the coverage should exceed -70 dBm. It was important that the suggested antennas provide the desired coverage. Therefore, this threshold was modified so that the probability of a predicted RSS value exceeding -70 dBm was 95%. At GH, the modified threshold was estimated to -63 dBm, as predicted values higher than this exceed -70 dBm with 95% certainty. Furthermore, it was desirable to minimize the number of antennas to reduce the costs of hardware and installation. A greedy search algorithm was proposed and implemented to suggest antenna locations that satisfy the requirements given the predictions.

To evaluate the result of the optimization algorithm, antennas were positioned in all possible combinations at GH and measurements were carried out for all target locations. The measurements revealed that two antennas would be sufficient and that multiple combinations would fulfil the requirements. The results of the optimization algorithm also suggested that two antennas would provide sufficient coverage and the suggested location matched one of the measured antenna alternatives. Hence, the optimization provides a satisfying solution.

However, the quality of the optimization is tightly linked to the quality of the estimation of the model parameters. At GH, the parameters are estimated from measurements obtained from the entire test site which yields a good set of parameters. Thus, this evaluation is carried out under ideal circumstances, but what would happen if the available measurements were fewer and obtained from random parts of the floor, e.g. if a limited area was available for measurements?

To answer this question the normality property of the residuals were utilized. Since the residuals can be considered normally distributed, it follows that the estimation of the parameters are normally distributed as well when using ordinary least squares. Thus, the variance can be calculated and depends on the number of samples. This information was used to simulate different scenarios where different parameters were utilized. The scenarios yielded different predictions which was then used to optimize the antennas. The number of times the optimization algorithm succeeded was recorded and compared to the total

number of times tested to estimate a probability of success. This revealed that there was approximately a 90% chance that the optimization algorithm could find the optimal solution at GH when measurements was collected all over the test site. When the number of measurements were dropped to half, on the other hand, the probability of success was approximately 75%.

6.2 Sources of uncertainty

6.2.1 Signal fading

The estimation of parameters has been shown to be vital to achieve good predictions and optimization results. High quality and comprehensive measurements lay a good foundation for sufficiently estimated parameters. Yet, a large amount of comprehensive measurements do not counteract measurement errors.

The measured received signal strength are characterized by its non-static manor, i.e., its tendency to fluctuate over time. Signal fading explains this random fluctuations. The sources of signal fading are many and a couple of relevant examples are given in this section.

Measuring received signal strength can be be a difficult task. It has been reported that the standard deviation can vary as much as 3 dBm when conducting measurements with a smart phone [13]. Furthermore, the radio propagation environment indoors is very sensitive. Multipath effects, i.e., the effect of two or more radio signals from the same source arriving at the destination using different paths, are a common phenomena indoors. Multipath may result in destructive interference that result in sudden fading, i.e., a sudden loss in signal power. This phenomenon might explain the small number of anomalies in the MH1 measurements. The attenuation in the corridor is generally decreasing rather smoothly as the distance from the transmitter increase. In a small number of measurements, however, this is not the case, figure 4.12a.

Multipath effects can also be caused by the human body. The technician that holds the smart phone will obstruct the signal and affect the received power dependent on if he or she is standing in the LOS direction of the radio wave or not. Variations of as much as 20 dBm caused solely by whether or not the body of a technician is placed between the reciever and the transmittor or not in a point has been reported [14].

6.2.2 Reusing parameters

One common assumption when using empirical models, such as the one-slope model, is that parameters, such as the path loss exponent, can be estimated at typical locations to then be reused at other similar locations. This allows predictions and optimization of sites without the need for collecting measurements. To test this methodology, another corridor, similar to the test site MH1, was selected in the Centre for Mathematical Sciences, figure 6.1. The walls had the same properties as the MH1 and the adjacent offices were about the same

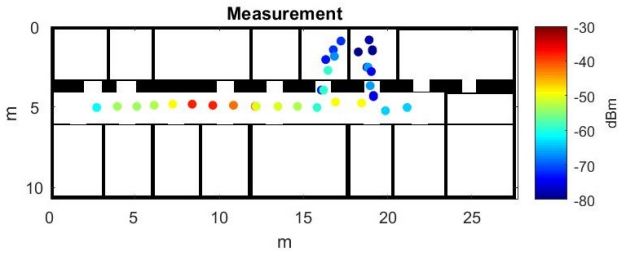

(a)

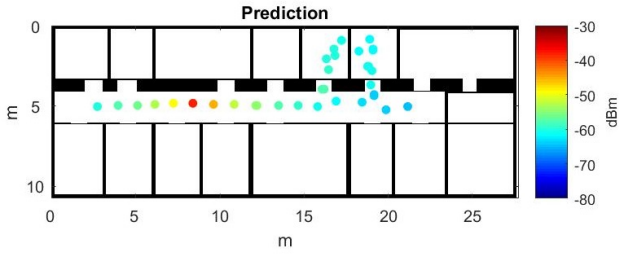

(b)

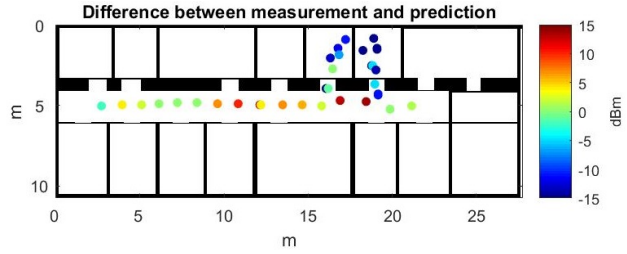

(c)

Figure 6.1: Predictions at a similar corridor as the test site MH1 reusing the model parameters from the latter. Figure (a) depicts the measurements, (b) the predicted values, and (c) the difference between measurement and prediction.

size. The dimensions of the corridor is roughly the same as MH1. Since no model performed significantly better than the other in the evaluation corridor the dual-slope model was selected because of its simplicity and speed.

The access point is mounted in the ceiling in the left part of the corridor. The offices located on the right side of the corridor have experienced poor coverage. To validate this claim, measurements were taken in the corridor as well as in the two offices where poor coverage has been reported. The result of the measurements clearly showed that the coverage is poor, i.e., around -80 dBm, in the two offices, figure 6.1a. To examine if it could be possible to predict the poor coverage without location specific measurement based parameter estimates, a prediction using the parameters from its sister corridor was conducted, as shown in figure 6.1b. The residuals in figure 6.1c reveals that the predictions in the two offices are bad, as it differ 15 dBm from the measured received signal strength. Thus, reusing parameters did not work sufficiently in this case.

6.2.3 Assumptions

Many assumptions and simplifications have been employed during this master's thesis. To begin with, all antennas are modelled as isotropic antennas, i.e., they distributes their signal energy equally in all directions, floor penetration is neglected etc. In fact, even the empirical models are making huge assumptions when they bundle all the information in just one exponent. Also using a regular smart phone for measuring the true received signal strength which is then used for the comparison for the predictions is also risky since the deviation of the measurements is high. All this contributes to error-prone results; this is a well known problem but as the option is often to guess antenna locations based on experience, it is still interesting how much could be said with the presented simple methods.

When finding the dominant paths, the material properties of the walls are important parameters in order to approximate the paths correctly. However, when calculating the paths, no such information was available. In the start of the project, it was our intent that such measurements were going to be done by a company in collaboration with this project. Unfortunately, the measurements were not performed in time and as a replacement standard values needed to be used. Therefore, the dominant paths might be approximated under wrong premisses in this thesis and will affect the accuracy of the predictions.

6.3 Convex optimization

The optimization problem in 5.18 was proposed to be solved using a greedy search algorithm. The greedy search algorithm is fast and easy to implement. Initially, the idea was to solve the optimization problem by relaxing it to a convex form to obtain a suboptimal solution but instead gain speed. The ℓ_0-(quasi) norm is non-convex, as is the constraint on the boolean set $\mathbf{w} \in \{0,1\}^M$ where M is the number of possible antenna locations. The relaxation is done by replacing the boolean constraint with the convex box constraint $[0,1]^M$. Furthermore, the non-convex ℓ_0-norm was replaced by a known efficient heuristic, namely the ℓ_1-norm. The optimization problem can then be formulated as

$$\mathbf{w}^* = \arg\min_{\mathbf{w}} ||\mathbf{w}||_1 \tag{6.1}$$

$$\text{s.t.} \quad \hat{\mathbf{T}}^T\mathbf{w} \geq \mathbb{1}_N \tag{6.2}$$

$$\mathbf{w} \in [0,1]^M \tag{6.3}$$

where the ℓ_1-norm is defined as

$$||\mathbf{w}||_1 \triangleq \sum_{m=1}^{M} |w_m|. \tag{6.4}$$

This optimization problem can be solved fast and efficiently using interior-point methods [5]. A solver implemented for Matlab to solve convex problem is the

CVX-solver. It was used to solve the optimization problem. However, this approach was abandoned in favour for the greedy search algorithm since it was hard to interpret the selection vector $\mathbf{w}$ when the box constraint was used. Normally, every component of $\mathbf{w}$ is rounded to nearest integer and that will be the final decision, but the constraint in (6.2) was not enough to push the solution over $\frac{1}{2}$, making it hard to decide on how many antennas to choose.

6.4 Conclusions

As mobile devices have become a vital part of peoples life, consumers expect mobile coverage indoors to make phone calls and browse the internet. Meanwhile, energy efficient houses makes it difficult or in some cases impossible for the radio waves to penetrate the walls. This raises the need for alternative solutions, such as indoor radio networks, in order to maintain sufficient coverage.

Network planning indoors is a difficult task. The possible locations to place antennas can be limited by practical and aesthetic reasons. It is often necessary to limit hardware cost due to budget restrains, consequently, minimizing the number of antennas. Indoor network planning is often performed on the basis of experience rather than utilizing prediction and optimization methods.

The main aim of this master's thesis was to propose an optimization algorithm that suggests the minimum number of antennas needed to fulfil a threshold requirement by selecting the best subset of all possible locations. To achieve this, a reasonable good prediction model is required. Both the prediction and optimization need to be fast in order to compete with experience based radio planning.

This master's thesis studied four different propagation models. The empirical one- and dual-slope models, the semi-deterministic dominant path model and, its dual-slope extension. These models were evaluated on three test sites with different characteristics. The models performed reasonably well. The dominant path models seemed to performed better than their straight path counterparts when the environment became more complex.

The optimization algorithm proposed was a greedy search algorithm. The approach was chosen for its simplicity and speed. The algorithm was able to find a sufficient solution for the test sites given the best performing prediction model. However, the result strongly depends on the model parameters which were estimated from measurements taken on the site. The parameters are intended to be calculated based on measurements taken on typical locations and then reused on a different site where measurements are not available to make predictions. However, a simple test showed that this is difficult and can yield erroneous results. Hence, the idea of making simulations and optimizations in buildings where measurements are not collected seems difficult. Nevertheless, the optimization part turned out to be rather accurate. If measurements were taken from all parts of the test site, it showed a 90% probability of finding an optimal solution if the path loss exponent is the only parameter unknown. If the reference parameter is unknown as well then the probability is around 80%. If measurements were only covering half the test site, the probabilities were

around 75% and 65%, respectively.

6.5 Further development

Modelling unmeasured buildings with empirical models seemed difficult. Nevertheless, if some measurements are available they can be used to suggest a design of an indoor radio network. For instance, a test antenna can be temporarily placed somewhere in the building and measurements can be collected to estimate the model parameters. These parameters can then be used to optimize the network and suggest antenna locations. These calculations are fast if using the models presented in this master's thesis, and can easily be implemented to run as an application on a mobile device. If research is further conducted on converting floor plans to the binary image format proposed in this thesis, the built-in camera of a mobile device could be used to photograph the floor plan and automatically convert it to the required format. Then, measurements can be collected and pinpointed using the application, and the optimization can be run on the same application as well.

There are plenty of propagation models not mentioned in this thesis. It would be interesting to research spatial statistical models that can fill in the blanks of a site survey.

Appendix A

Additional plots

A.1 Plots for GH

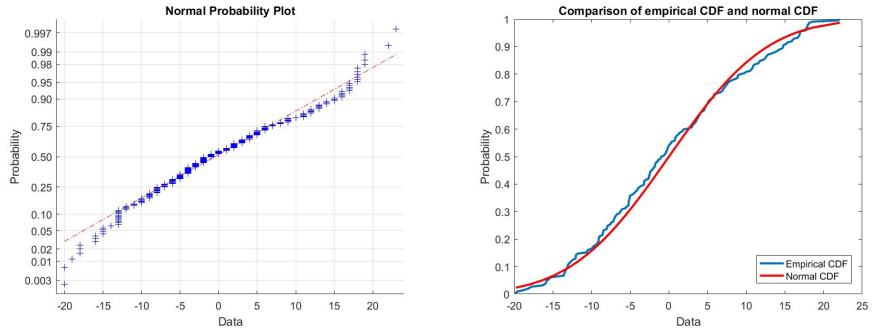

(a) (b)

Figure A.1: In (a), normal probability plot for the residuals of the one-slope model at GH. In (b), the empirical cumulative distribution function (blue) of the residuals compared to the estimated cumulative distribution function (red).

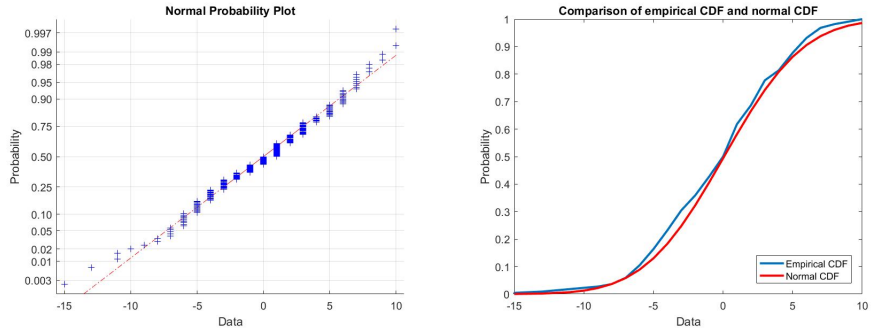

(a) (b)

Figure A.2: In (a), normal probability plot for the residuals of the dual-slope model at GH. In (b), the empirical cumulative distribution function (blue) of the residuals compared to the estimated cumulative distribution function (red).

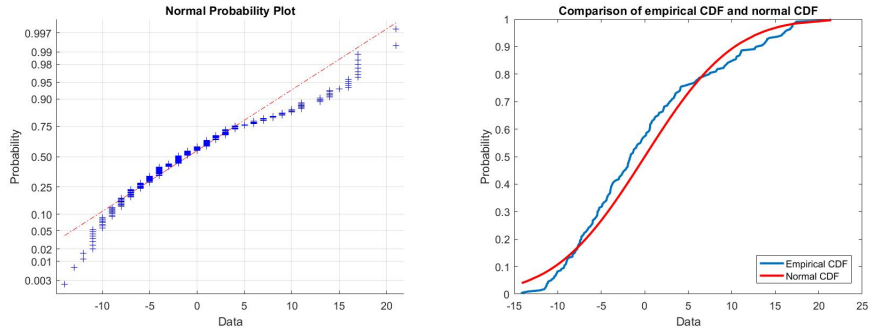

(a) (b)

Figure A.3: In (a), normal probability plot for the residuals of the dominant path model at GH. In (b), the empirical cumulative distribution function (blue) of the residuals compared to the estimated cumulative distribution function (red).

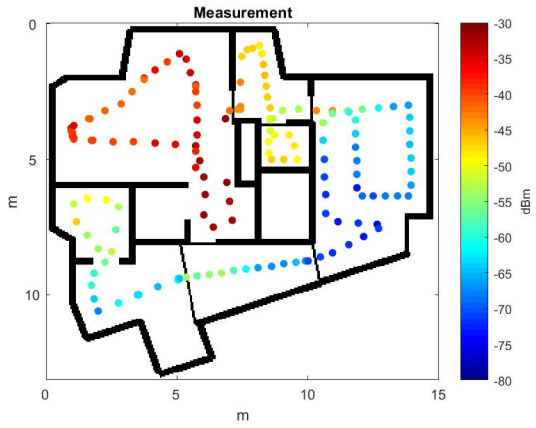

(a)

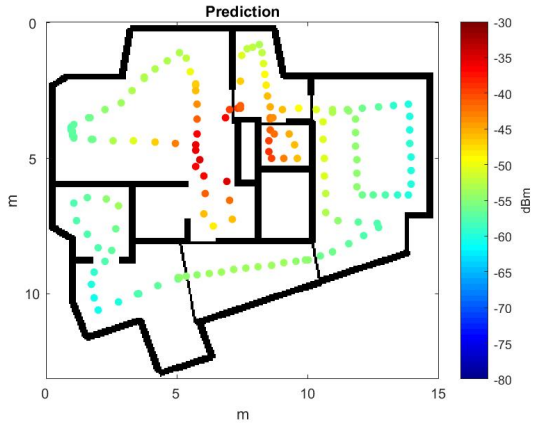

(b)

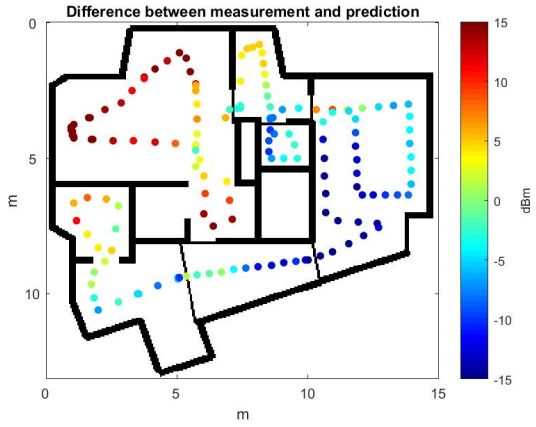

(c)

Figure A.4: Predictions at GH using the one-slope model. Figure (a) depicts the measurements, (b) the predicted values, and (c) the residuals between measurement and prediction.

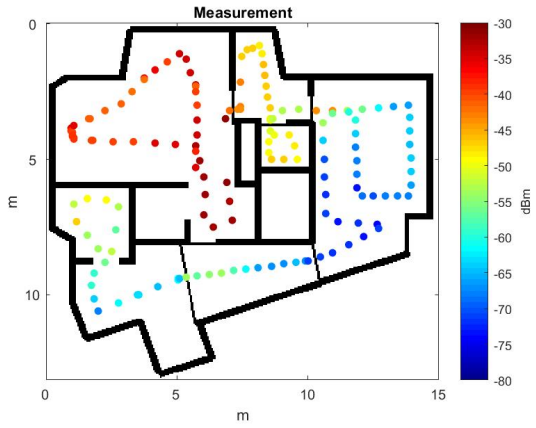

(a)

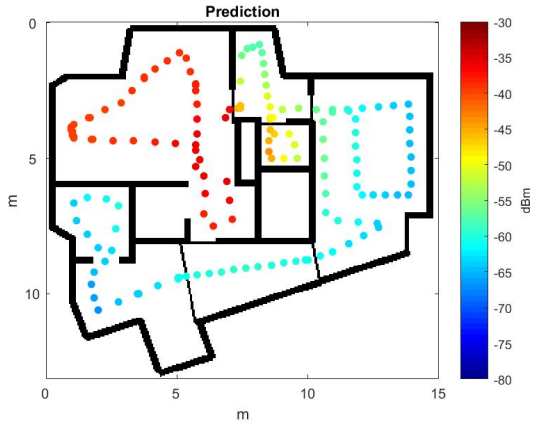

(b)

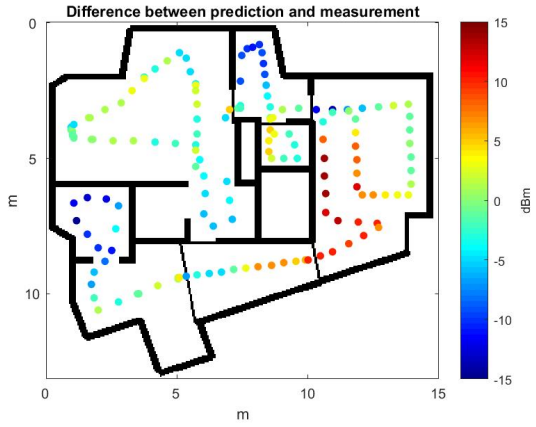

(c)

Figure A.5: Predictions at GH using the dual-slope model. Figure (a) depicts the measurements, (b) the predicted values, and (c) the residuals between measurement and prediction.

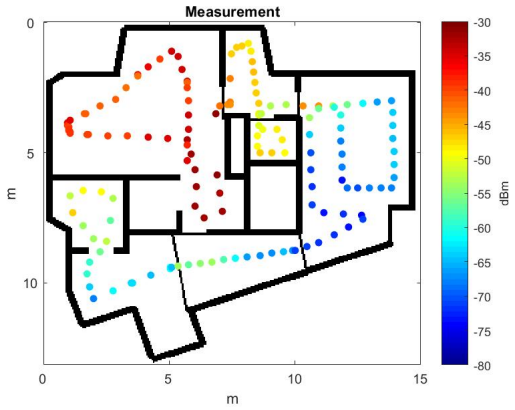

(a)

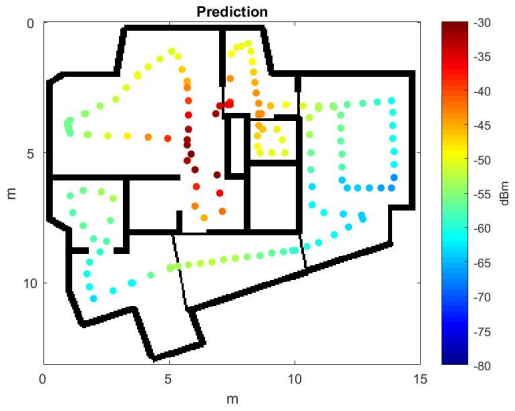

(b)

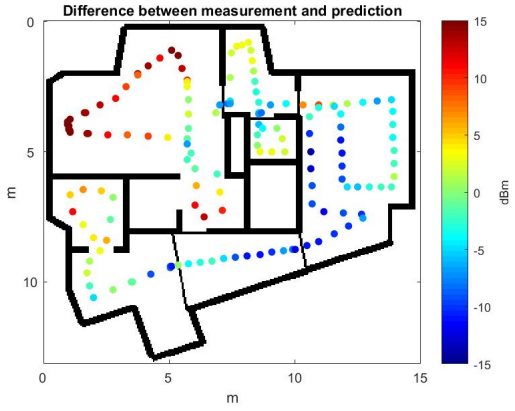

(c)

Figure A.6: Predictions at GH using the dominant path model. The paths were calculated using the A* search algorithm. Figure (a) depicts the measurements, (b) the predicted values, and (c) the difference between measurement and prediction.

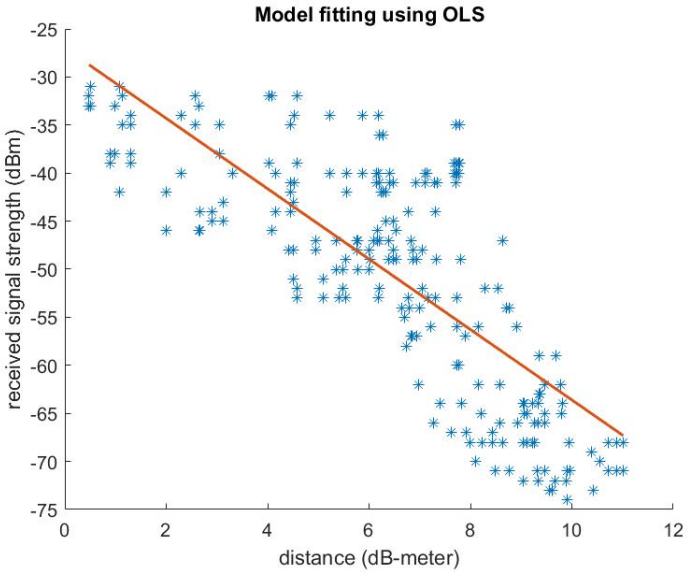

Figure A.7: The dominant path model fitted to measurement data collected at GH using ordinary least squares. The paths were retrieved using the Θ^* search algorithm.

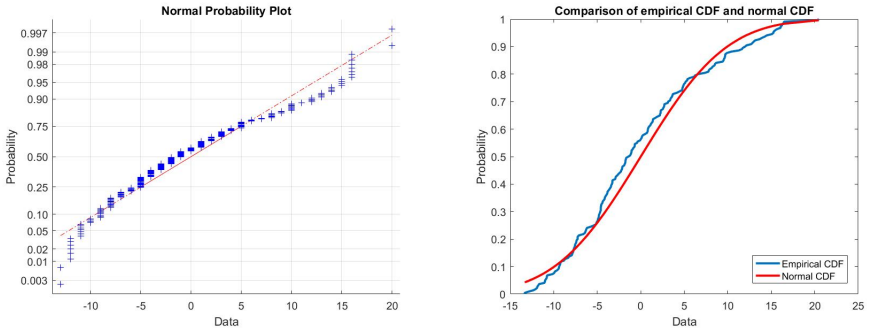

(a) (b)

Figure A.8: In (a), normal probability plot for the residuals of the dominant path model using the Θ^* search algorithm at GH. In (b), the empirical cumulative distribution function (blue) of the residuals compared to the estimated cumulative distribution function (red).

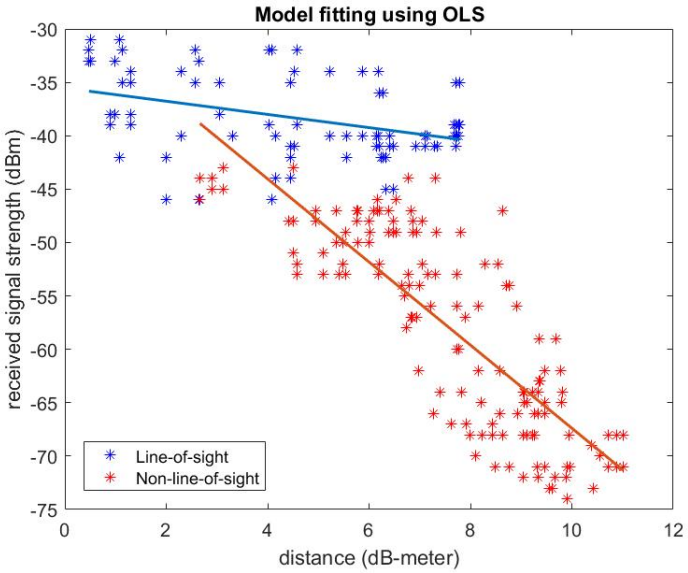

Figure A.9: The dual-slope dominant path model fitted to measurement data from GH using ordinary least square method. The paths were retrieved using the Θ^* search algorithm.

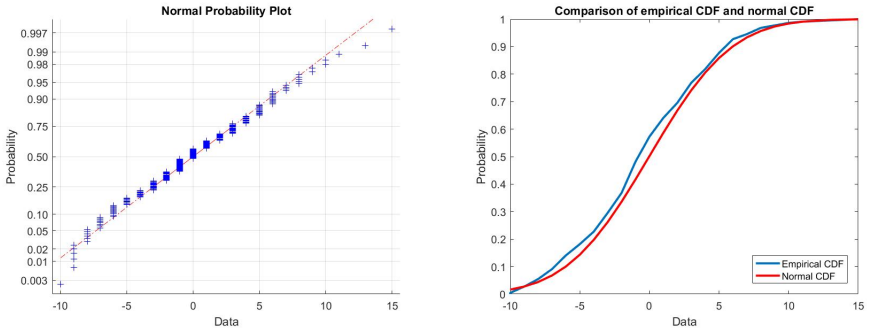

(a) (b)

Figure A.10: In (a), normal probability plot for the residuals of the dual slope dominant path model using the Θ^* search algorithm at GH. In (b), the empirical cumulative distribution function (blue) of the residuals compared to the estimated cumulative distribution function (red).

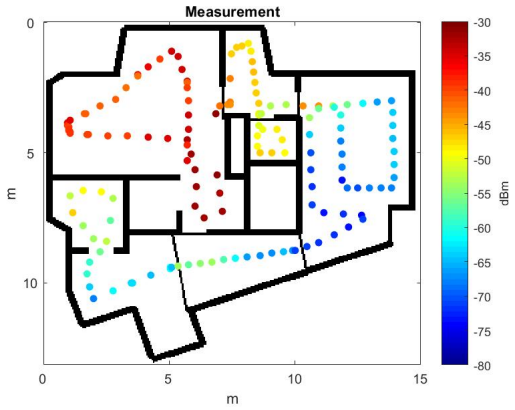

(a)

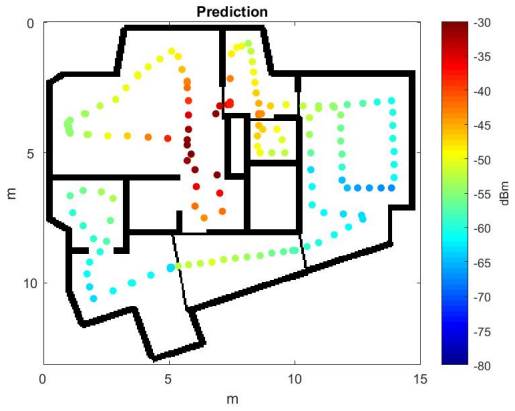

(b)

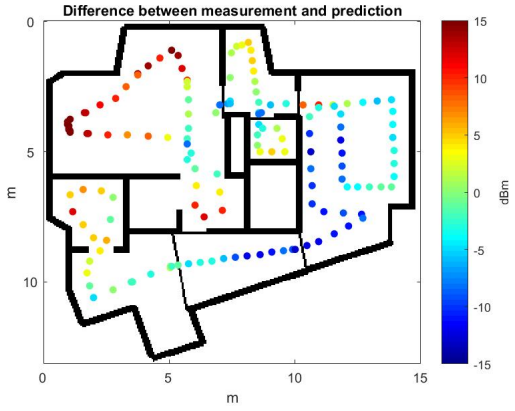

(c)

Figure A.11: Predictions at GH using the dominant path model. The paths were calculated using the Θ^* search algorithm. Figure (a) depicts the measurements, (b) the predicted values and (c) the difference between measurement and prediction.

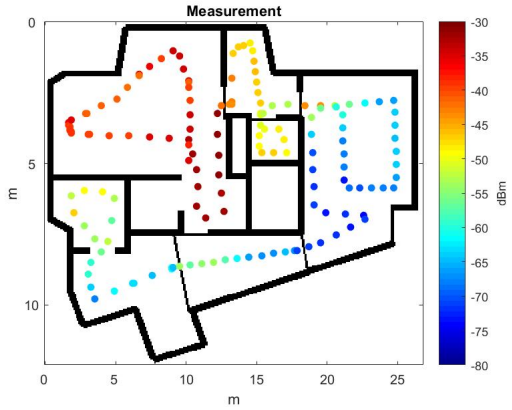

(a)

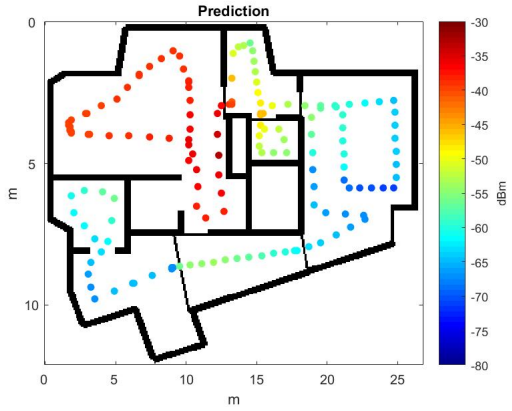

(b)

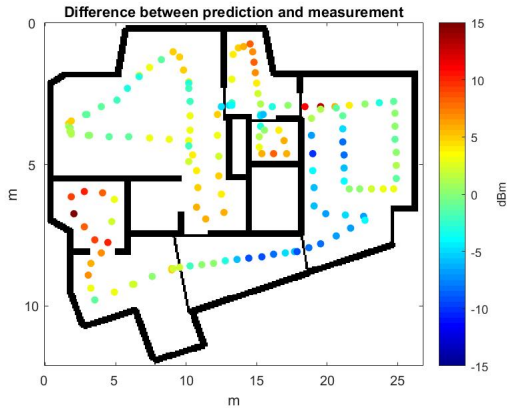

(c)

Figure A.12: Predictions at GH using the dual-slope dominant path model. The paths were calculated using the Θ^* search algorithm. Figure (a) depicts the measurements, (b) the predicted values and (c) the difference between measurement and prediction.

A.2 Plots for MH1

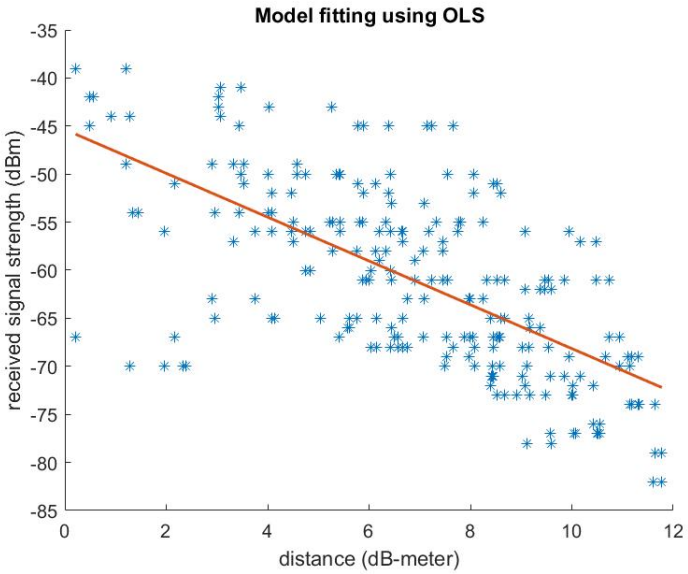

Figure A.13: The one-slope model fitted to measurement data from MH1 using ordinary least square method.

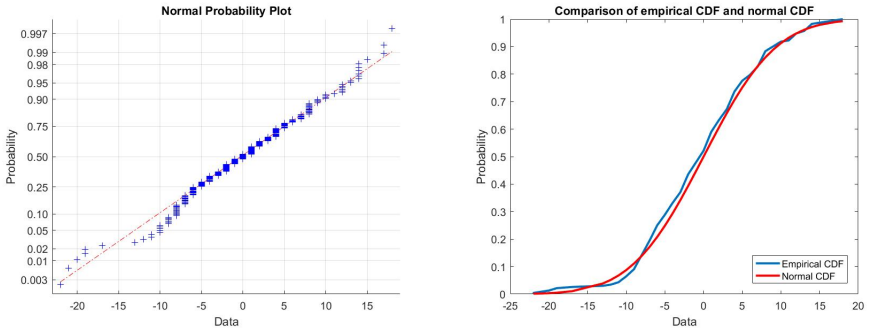

(a) (b)

Figure A.14: In (a), normal probability plot for the residuals of the one-slope model at MH1. In (b), the empirical cumulative distribution function (blue) of the residuals compared to the estimated cumulative distribution function (red).

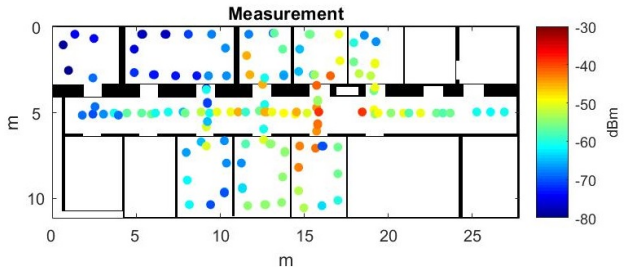

(a)

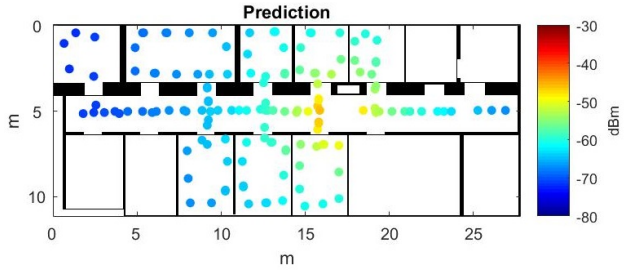

(b)

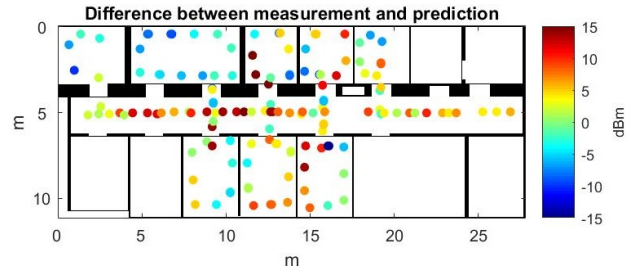

(c)

Figure A.15: Predictions at MH1 using the one-slope model. Figure (a) depicts the measurements, (b) the predicted values and (c) the difference between measurement and prediction.

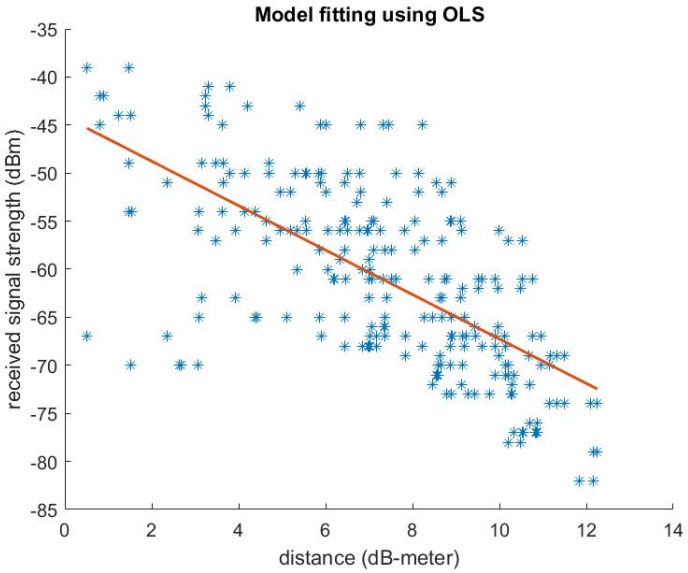

Figure A.16: The dominant path model fitted to measurement data from MH1 using ordinary least square method. The paths were retrieved using the A* search algorithm.

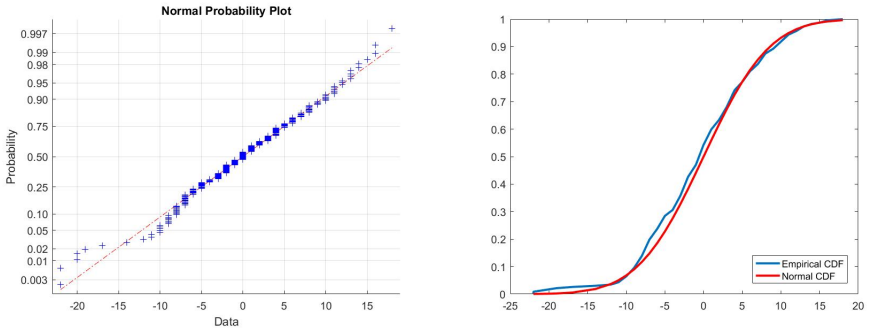

(a) (b)

Figure A.17: In (a), normal probability plot for the residuals of the dominant path model using the A* search algorithm at MH1. In (b), the empirical cumulative distribution function (blue) of the residuals compared to the estimated cumulative distribution function (red).

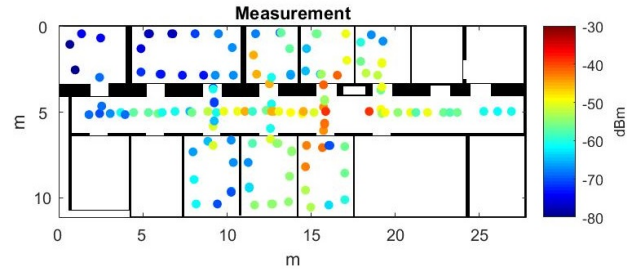

(a)

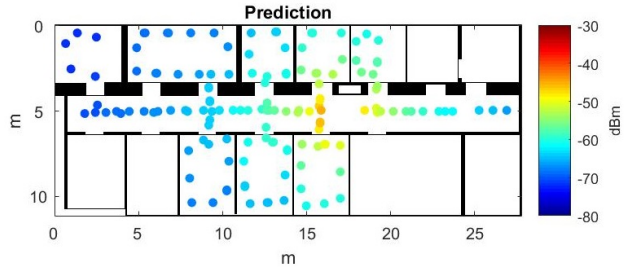

(b)

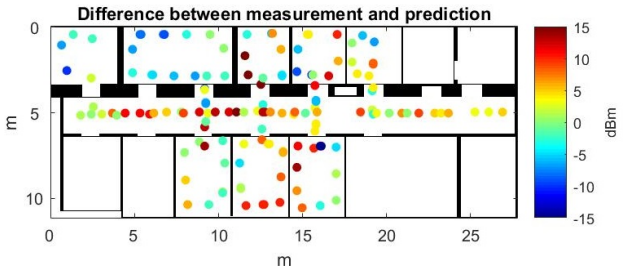

(c)

Figure A.18: Predictions at MH1 using the dominant path model. The paths were calculated using the A* search algorithm. Figure (a) depicts the measurements, (b) the predicted values and (c) the difference between measurement and prediction.

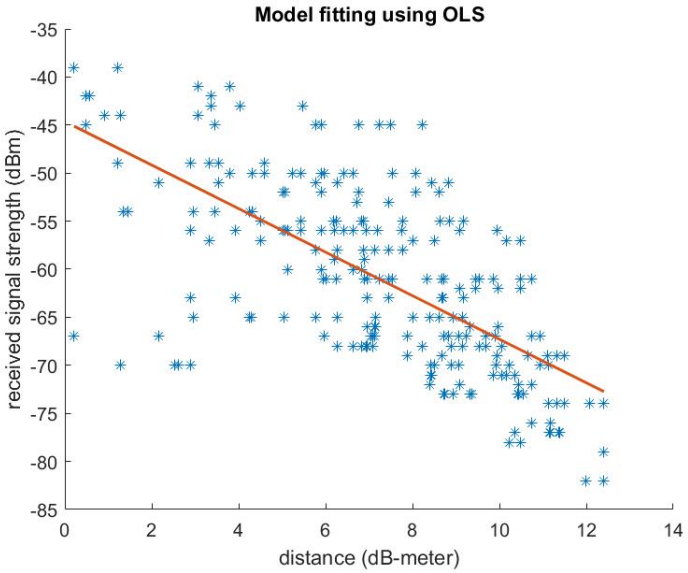

Figure A.19: The dominant path model fitted to measurement data from MH1 using ordinary least square method. The paths were retrieved using the Θ^* search algorithm.

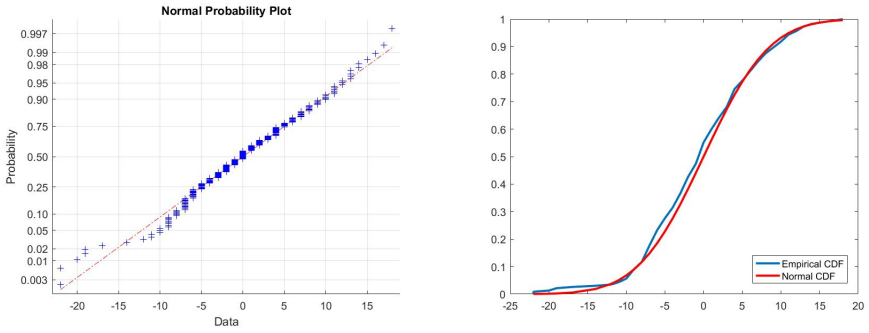

(a) (b)

Figure A.20: In (a), normal probability plot for the residuals of the dominant path model using the Θ^* search algorithm at MH1. In (b), the empirical cumulative distribution function (blue) of the residuals compared to the estimated cumulative distribution function (red).

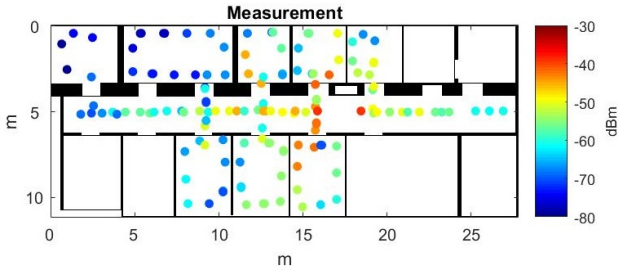

(a)

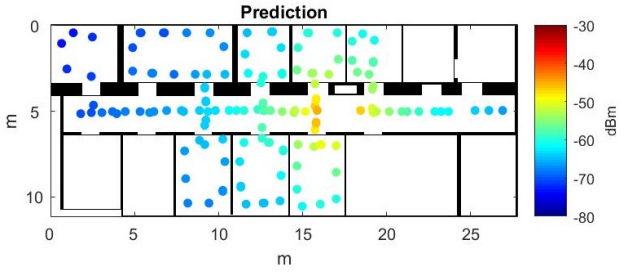

(b)

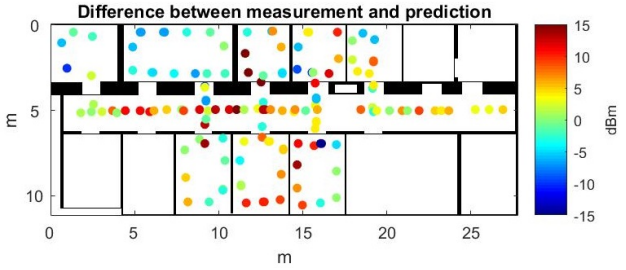

(c)

Figure A.21: Predictions at MH1 using the dominant path model. The paths were calculated using the Θ^* search algorithm. Figure (a) depicts the measurements, (b) the predicted values and (c) the difference between measurement and prediction.

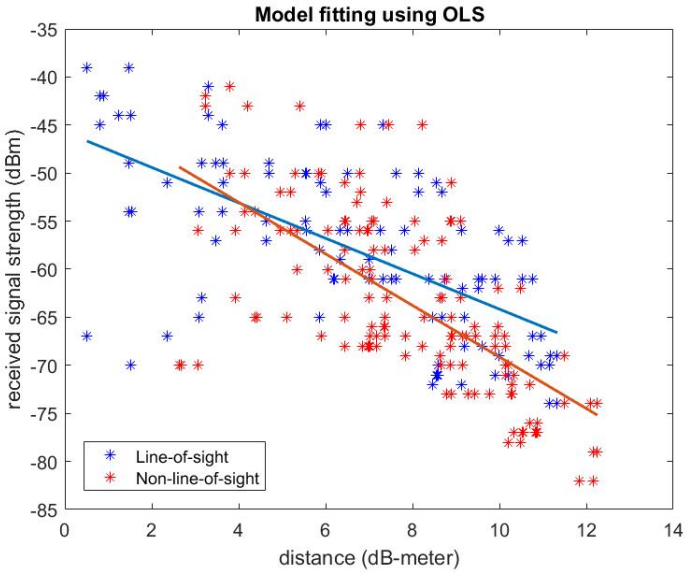

Figure A.22: The dual-slope dominant path model fitted to measurement data from MH1 using ordinary least square method. The paths were retrieved using the A* search algorithm.

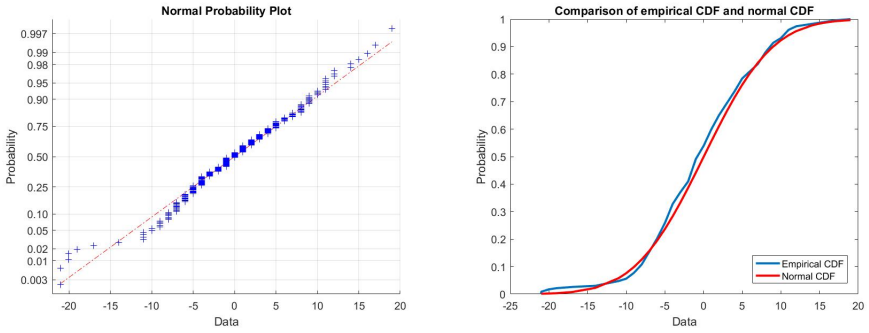

(a) (b)

Figure A.23: In (a), normal probability plot for the residuals of the dual-slope dominant path model using the A* search algorithm at MH1. In (b), the empirical cumulative distribution function (blue) of the residuals compared to the estimated cumulative distribution function (red).

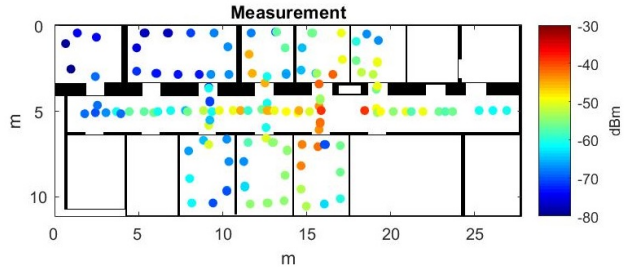

(a)

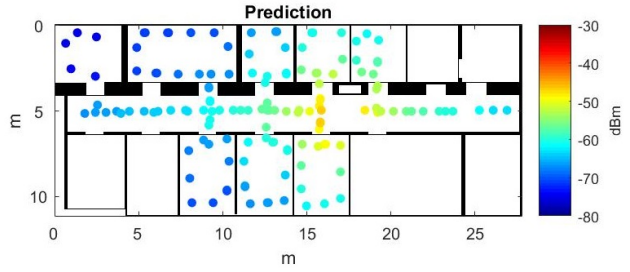

(b)

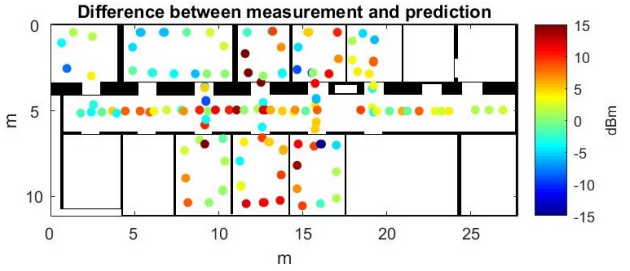

(c)

Figure A.24: Predictions at MH1 using the dual-slope dominant path model. The paths were calculated using the A* search algorithm. Figure (a) depicts the measurements, (b) the predicted values and (c) the difference between measurement and prediction.

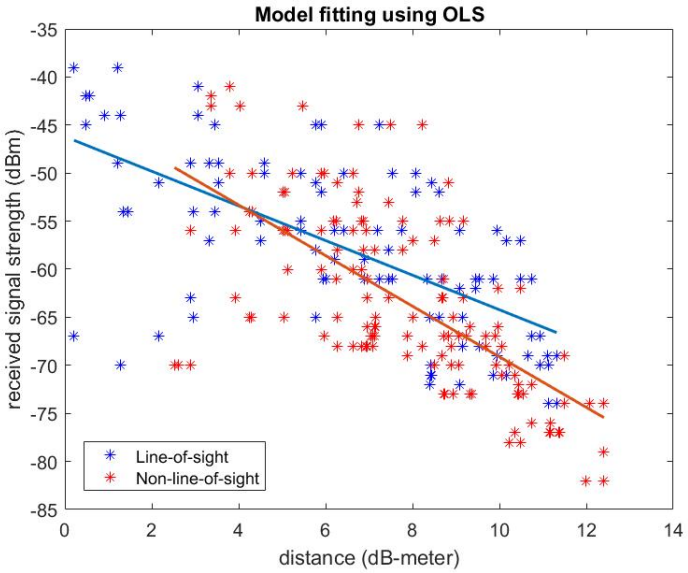

Figure A.25: The dual-slope dominant path model fitted to measurement data from MH1 using ordinary least square method. The paths were retrieved using the Θ^* search algorithm.

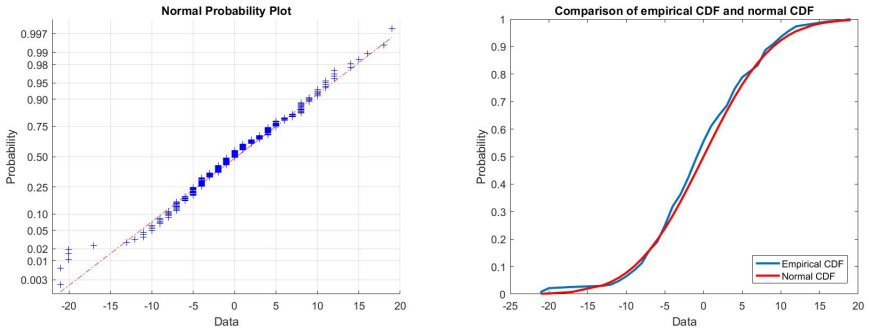

(a) (b)

Figure A.26: In (a), normal probability plot for the residuals of the dual-slope dominant path model using the Θ^* search algorithm at MH1. In (b), the empirical cumulative distribution function (blue) of the residuals compared to the estimated cumulative distribution function (red).

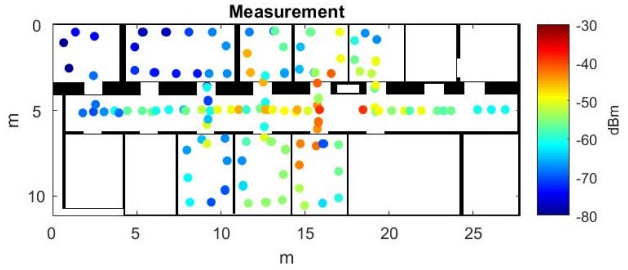

(a)

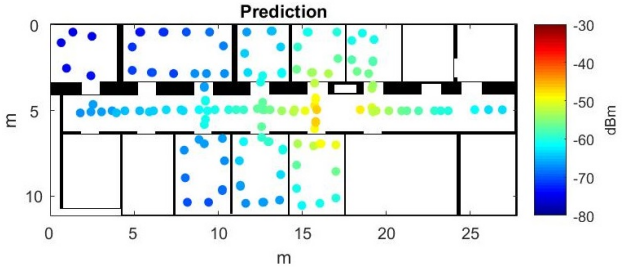

(b)

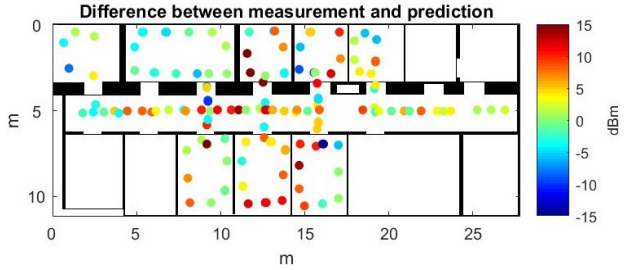

(c)

Figure A.27: Predictions at MH1 using the dual-slope dominant path model. The paths were calculated using the Θ^* search algorithm. Figure (a) depicts the measurements, (b) the predicted values and (c) the difference between measurement and prediction.

A.3 Plots for MH2

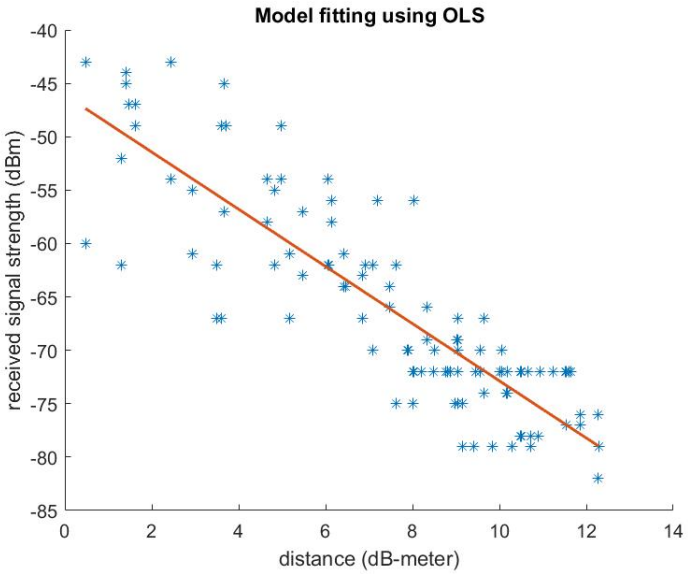

Figure A.28: The one-slope model fitted to measurement data from MH2 using ordinary least square method.

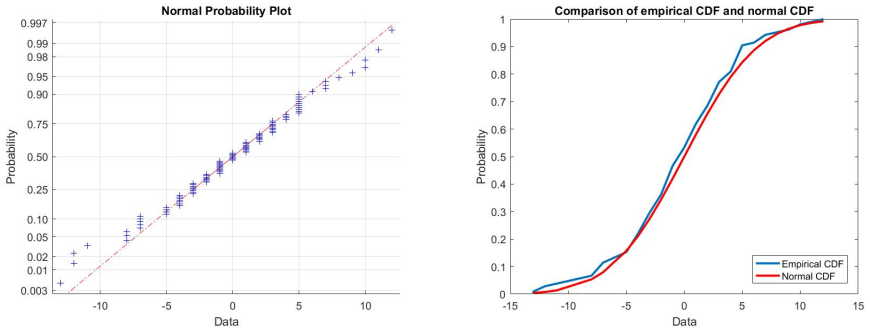

(a) (b)

Figure A.29: In (a), normal probability plot for the residuals of the one-slope model at MH2. In (b), the empirical cumulative distribution function (blue) of the residuals compared to the estimated cumulative distribution function (red).

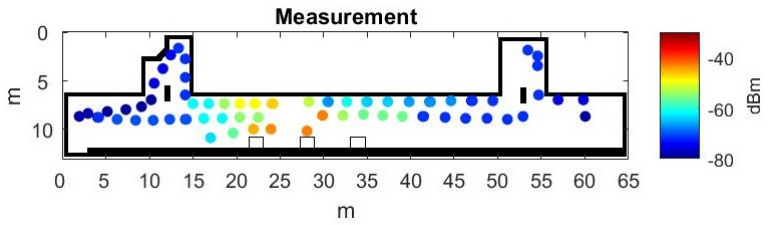

(a)

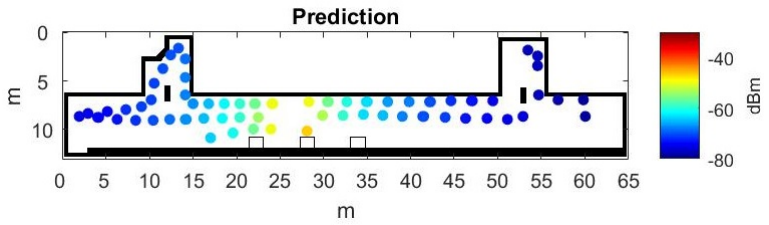

(b)

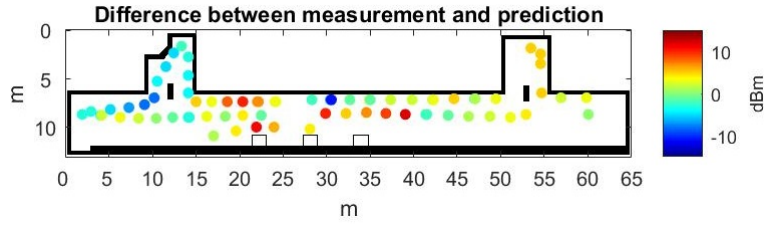

(c)

Figure A.30: Predictions at MH2 using the one-slope model. Figure (a) depicts the measurements, (b) the predicted values and (c) the difference between measurement and prediction.

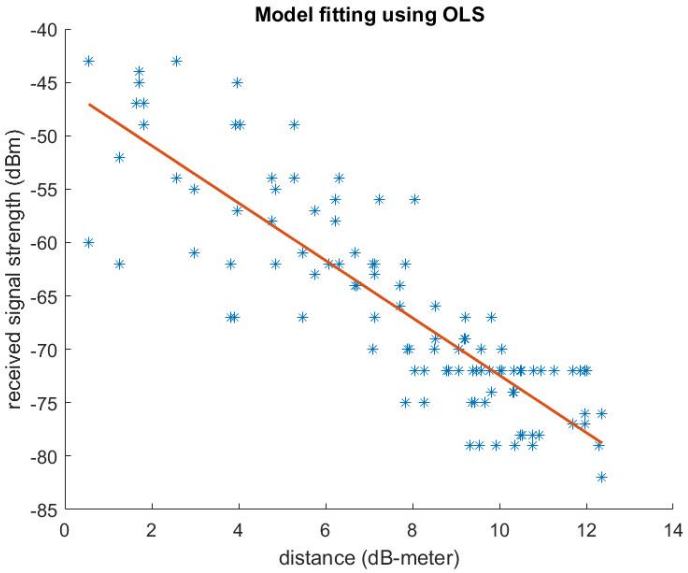

Figure A.31: The dominant path model fitted to measurement data from MH2 using ordinary least square method. The paths were retrieved using the A* search algorithm.

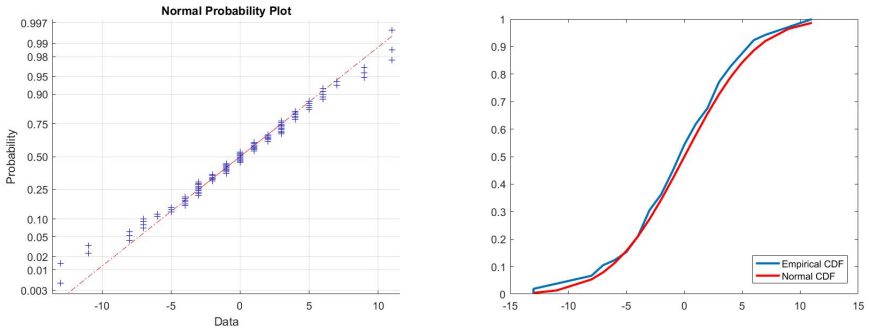

(a) (b)

Figure A.32: In (a), normal probability plot for the residuals of the dominant path model using the A* search algorithm at MH2. In (b), the empirical cumulative distribution function (blue) of the residuals compared to the estimated cumulative distribution function (red).

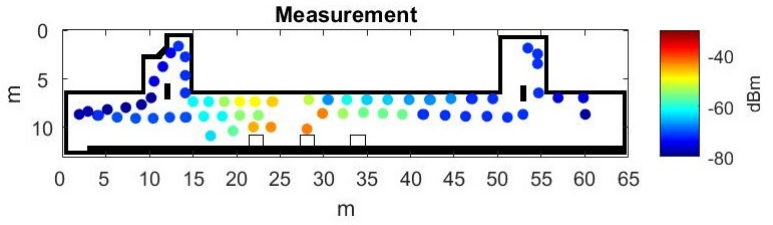

(a)

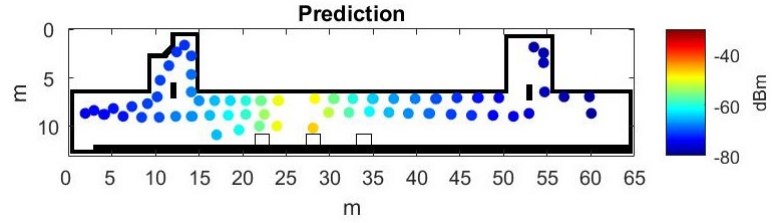

(b)

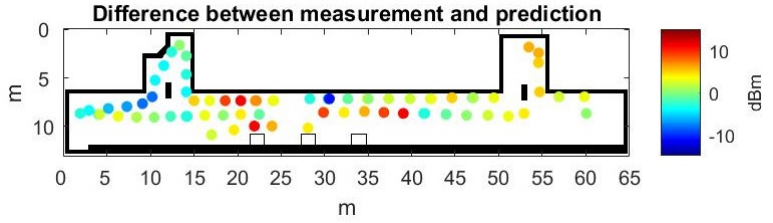

(c)

Figure A.33: Predictions at MH2 using the dominant path model. The paths were calculated using the A* search algorithm. Figure (a) depicts the measurements, (b) the predicted values and (c) the difference between measurement and prediction.

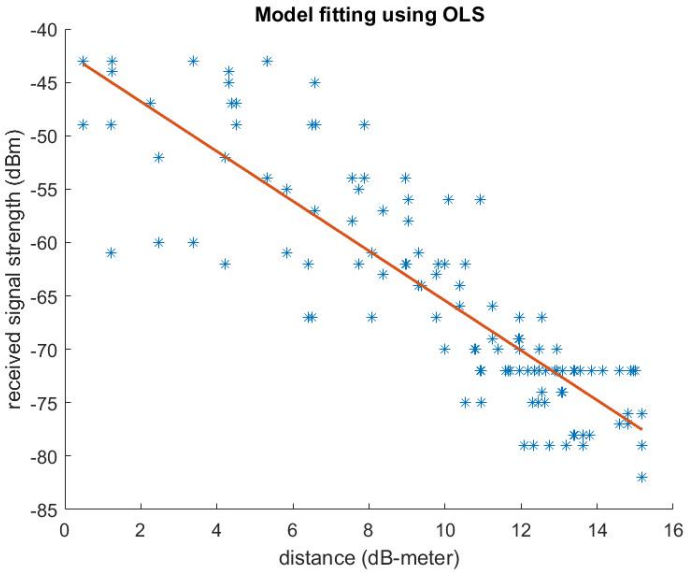

Figure A.34: The dominant path model fitted to measurement data from MH2 using ordinary least square method. The paths were retrieved using the Θ^* search algorithm.

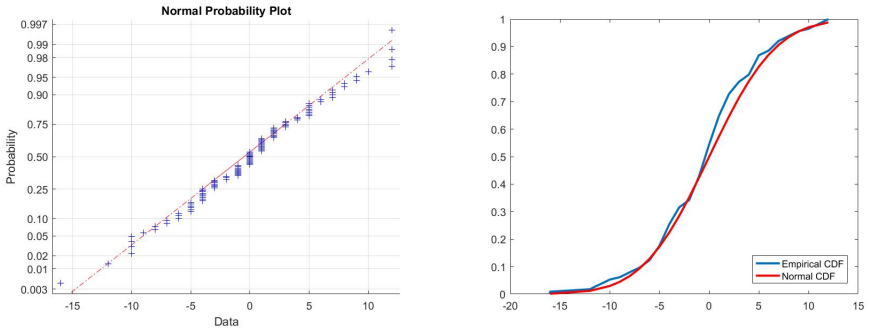

(a) (b)

Figure A.35: In (a), normal probability plot for the residuals of the dominant path model using the Θ^* search algorithm at MH2. In (b), the empirical cumulative distribution function (blue) of the residuals compared to the estimated cumulative distribution function (red).

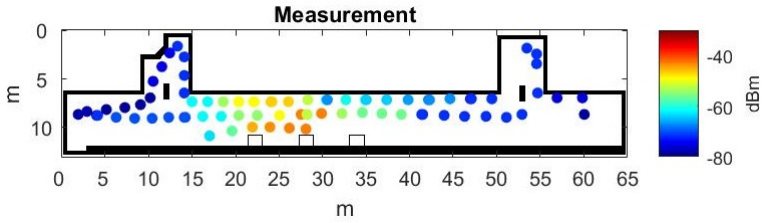

(a)

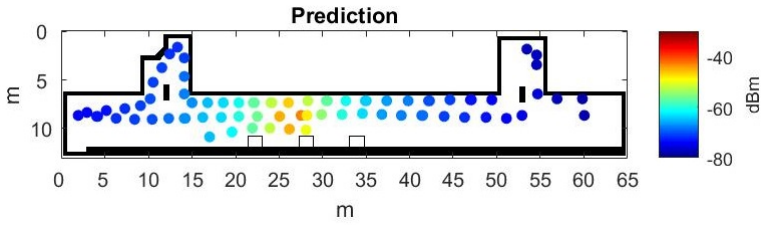

(b)

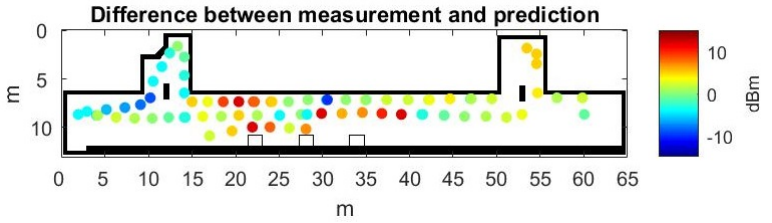

(c)

Figure A.36: Predictions at the MH2 using the dominant path model. The paths were calculated using the Θ^* search algorithm. Figure (a) depicts the measurements, (b) the predicted values and (c) the difference between measurement and prediction.

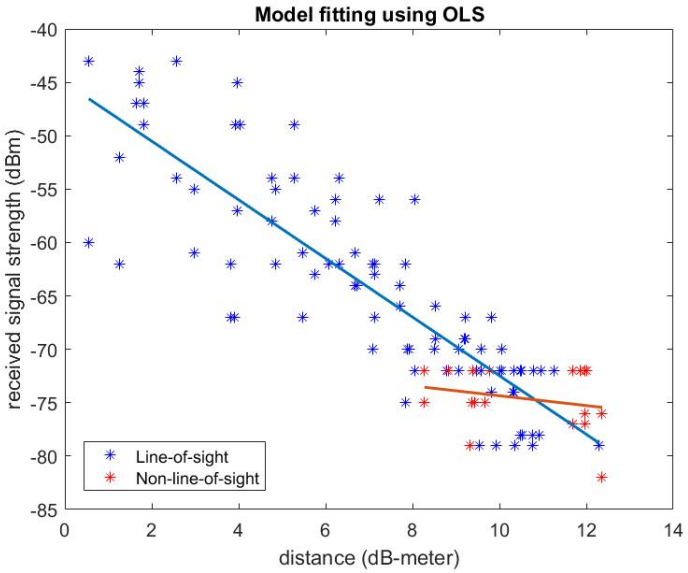

Figure A.37: The dual-slope dominant path model fitted to measurement data from MH2 using ordinary least square method. The paths were retrieved using the A* search algorithm.

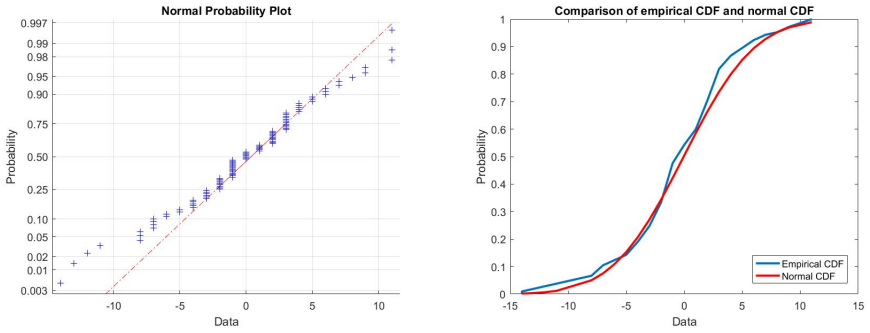

(a) (b)

Figure A.38: In (a), normal probability plot for the residuals of the dual-slope dominant path model using the A* search algorithm at MH2. In (b), the empirical cumulative distribution function (blue) of the residuals compared to the estimated cumulative distribution function (red).

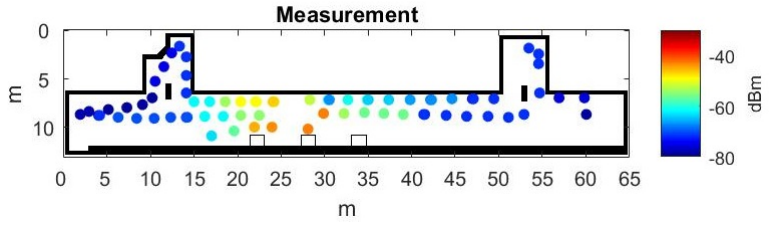

(a)

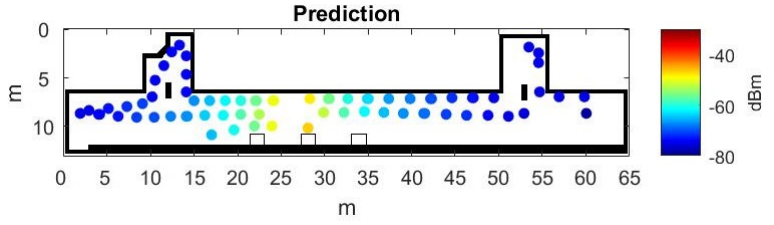

(b)

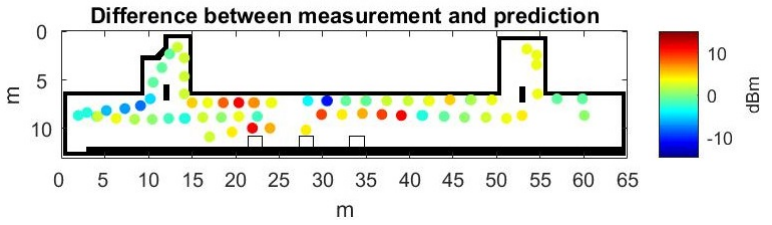

(c)

Figure A.39: Predictions at MH2 using the dual-slope dominant path model. The paths were calculated using the A* search algorithm. Figure (a) depicts the measurements, (b) the predicted values and (c) the difference between measurement and prediction.

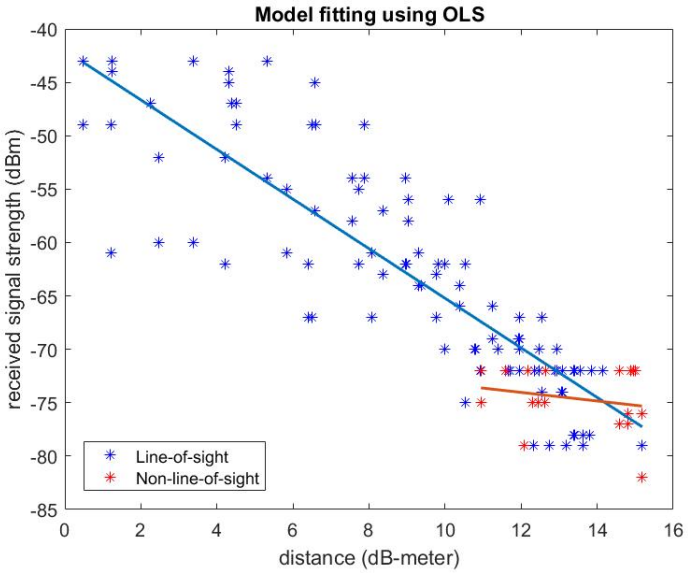

Figure A.40: The dual-slope dominant path model fitted to measurement data from MH2 using ordinary least square method. The paths were retrieved using the Θ^* search algorithm.

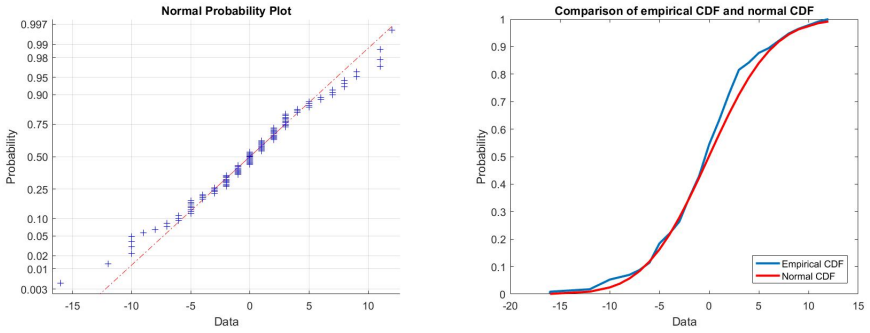

(a) (b)

Figure A.41: In (a), normal probability plot for the residuals of the dual-slope dominant path model using the Θ^* search algorithm at MH2. In (b), the empirical cumulative distribution function (blue) of the residuals compared to the estimated cumulative distribution function (red).

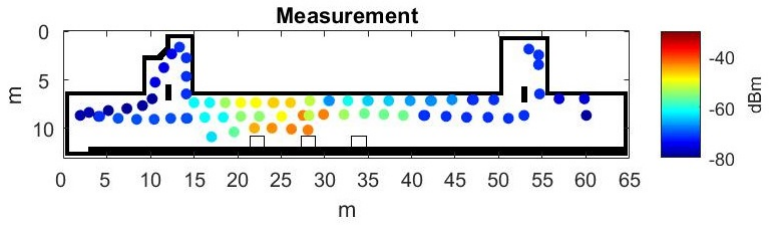

(a)

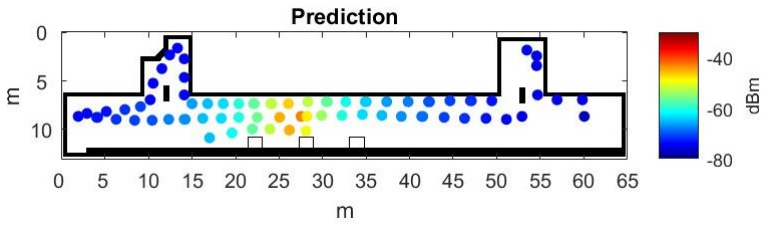

(b)

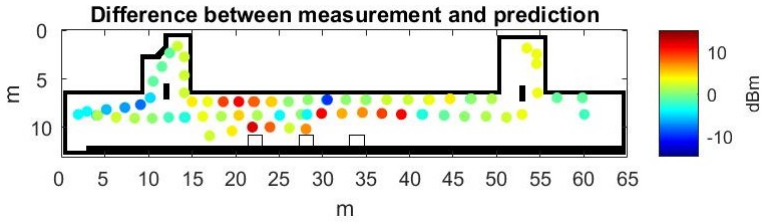

(c)

Figure A.42: Predictions at MH2 using the dual-slope dominant path model. The paths were calculated using the Θ^* search algorithm. Figure (a) depicts the measurements, (b) the predicted values and (c) the difference between measurement and prediction.

Bibliography

[1] PTS åtgärder för ökad mobiltäckning. Technical Report Dnr: 14-7016, Post- och telestyrelsen, Stockholm, Sweden, June 2014.

[2] PTSFS 2012:3. Post- och telestyrelsens författningssamling, September 2012.

[3] S. Šain. Modelling and characterization of wireless channels in harsh environments. Master's thesis, Mälardalen University, June 2011.

[4] Y. Chen and A. Terzis. On the implications of the log-normal path loss model: An efficient method to deploy and move sensor motes, November 2011.

[5] S. Prabhakar Chepuri and G. Leus. Sparsity-promoting sensor selection for non-linear measurement models. *IEEE Transactions on Signal Processing*, 3:684–698, February 2015.

[6] M. Chiang. A* optimality proof, cycle checking. `https://www.cs.ubc.ca/~hutter/teaching/cpsc322/2-Search5.pdf`. Accessed: 2017-03-27.

[7] Wikimedia Commons. File:sample floorplan.jpg. `https://commons.wikimedia.org/wiki/File:Sample_Floorplan.jpg`. Accessed: 2017-03-27.

[8] E.W. Dijkstra. A note on two problems in connexion with graphs. *Numerische Mathematik*, 1:269–271, 1959.

[9] C. Perez-Vegay et al. A simple and efficient model for indoor path-loss prediction. *Meas. Sci. Technol*, 8:1166–1173, May 1997.

[10] G. Wölfle et al. Dominant path prediction model for indoor scenarios. *GeMiC*, pages 176–179, April 2005.

[11] K. Daniel et al. Theta*: Any-angle path planning on grids, September 2010.

[12] L. Norell et al. Wi-fi calling – extending the reach of volte to wi-fi. *Ericsson Review*, January 2015.

[13] Y. Zhuanget et al. Smartphone-based indoor localization with bluetooth low energy beacons. *Sensors — Open Access Journal*, May 2016.

[14] D. Zinkiewicz J. Rapiński and T. Stanislawek. Sinfluence of human body on radio signal strength indicator readings in indoor positioning systems. *Technical Sciences*, page 117–127, March 2016.

[15] L. Vuokko J. Salo and P. Vainikainen. Why is shadow fading lognormal? *Proc. International Symposium on Wire less Personal Multimedia Communications*, pages 522–526, September 2005.

[16] A. Jakobsson. *An Introduction to Time Series Modeling*. Studentlitteratur, November 2015.

[17] M. Luo. Indoor radio propagation modeling for system performance prediction, January 2013.

[18] Mathuranathan. Log distance path loss or log normal shadowing model, September 2013.

[19] K. Mella. Theory, simulation and measurement of wireless multipath fading channels, May 2007.

[20] S. Mussmann and A. See. Graph search algorithms. `http://cs.stanford.edu/people/abisee/gs.pdf`. Accessed: 2017-03-27.

[21] N. J. Nilsson P. E. Hart and B. Raphael. A formal basis for the heuristic determination of minimum cost paths. *IEEE Transactions on Systems Science and Cybernetics*, 4:100–107, July 1968.

[22] J.A. Shaw. Radiometry and the friis transmission equation. *American Journal of Physics*, 8:33–37, January 2013.

[23] G. Soldi. Wireless positioning using ellipsoidal constraints. Master's thesis, Lund University, June 2011.

[24] European Union. Directive 2010/31/eu of the european parliament and of the council on the energy performance of buildings, November 2016.

[25] J. Wännström. Inomhustäckning – sammanställning av lösningar. Technical Report PTS-ER-2015:12, Post- och telestyrelsen, Stockholm, Sweden, May 2015.

[26] G. Woelfle and F.M. Landstorfer. Dominant paths for the field strength prediction,. *48th IEEE Vehicular Technology Conference (VTC) 1998*, pages 552–556, May 1998.

[27] M. Li Y. Zhao and F. Shi. Indoor radio propagation model based on dominant path. *Int. J. Communications, Network and System Sciences*, pages 330–337, March 2010.